

Annual Review of Nuclear and Particle Science From Nuclei to the Cosmos: Tracing Heavy-Element Production with the Oldest Stars

Anna Frebel

Department of Physics and Kavli Institute for Astrophysics and Space Research, Massachusetts Institute of Technology, Cambridge, Massachusetts 02139, USA; email: afrebel@mit.edu

Annu. Rev. Nucl. Part. Sci. 2018. 68:237-69

First published as a Review in Advance on July 25, 2018

The Annual Review of Nuclear and Particle Science is online at nucl.annualreviews.org

https://doi.org/10.1146/annurev-nucl-101917-021141

Copyright © 2018 by Annual Reviews. All rights reserved

ANNUAL CONNECT

www.annualreviews.org

- Download figures
- Navigate cited references
- · Keyword search
- · Explore related articles
- · Share via email or social media

Keywords

Milky Way Galaxy, stellar chemical abundances, metal-poor stars, dwarf galaxies, nucleosynthesis, early Universe

Abstract

Understanding the origin of the elements has been a decades-long pursuit, with many open questions remaining. Old stars found in the Milky Way and its dwarf satellite galaxies can provide answers because they preserve clean element abundance patterns of the nucleosynthesis processes that operated some 13 billion years ago, enabling reconstruction of the chemical evolution of the elements. This review focuses on the astrophysical signatures of heavy neutron-capture elements made in the s-, i-, and r-processes found in old stars. A highlight is the recently discovered r-process galaxy Reticulum II, which was enriched by a neutron star merger. These results show that old stars in dwarf galaxies provide a novel means to constrain the astrophysical site of the r-process, ushering in much-needed progress on this major outstanding question. This nuclear astrophysics research complements the many experimental and theoretical nuclear physics efforts into heavy-element formation, and also aligns with results on the gravitational-wave signature of neutron star mergers.

Contents 1.1. From Nuclei to the Cosmos: The Oldest Stars as Probes of the Early Universe 238 2. CHEMICAL ABUNDANCE MEASUREMENTS OF OLD 3. SIGNATURES OF NEUTRON-CAPTURE ELEMENTS 4.4. Chemical Evolution of Neutron-Capture Elements and the Galaxy

I ask you to look both ways. For the road to a knowledge of the stars leads through the atom; and important knowledge of the atom has been reached through the stars.

-Sir Arthur Eddington, Lecture 1, Stars and Atoms (1928)

1. INTRODUCTION

The discovery that stars are made primarily from hydrogen and helium (1) led many scientists to realize that the study of the elements is intimately connected to the understanding of stars and their evolution (2). Nearly 100 years later, this research systematically continues, driven by stellar observations, nuclear physics experiments, and theoretical investigations to uncover the many interdisciplinary connections that will eventually lead to a more complete understanding of the cosmic origin of the chemical elements.

1.1. From Nuclei to the Cosmos: The Oldest Stars as Probes of the Early Universe

This decade has witnessed a tremendous increase in observational surveys and theoretical studies of our Milky Way Galaxy. In this so-called Galactic Renaissance, it is now widely recognized that detailed knowledge of the assembly history of the Milky Way and its satellite dwarf galaxies provides important constraints on our understanding of a wide variety of topics, ranging from nuclear physics and nuclear astrophysics to stellar astronomy, galaxy formation, and even observational cosmology. Studying the Milky Way and its stars and stellar populations also enables a complementary approach to observing the most distant galaxies that formed less than a billion years after the Big Bang, for instance, with NASA's James Webb Space Telescope. Ancient, undisturbed,

13-billion-year-old stars are now regularly found in our own Galaxy, and provide the opportunity to look back in time—right into the era of the very first stars—and elucidate the nucleosynthetic pathways to the formation of the elements, and the beginning of the chemical evolution that continues to this day.

The early history of the 13.8-billion-year-old Universe is encoded in the chemical compositions of ancient, low-mass $[M < 0.8 \text{ solar mass } (M_{\odot})]$ stars. Even today, the atmospheres of these still-shining stars reflect the composition of their birth gas clouds at the time and place of their formation some 13 billion years ago. They formed from the nearly pristine gas left over after the Big Bang, when the Universe was just starting to be enriched in elements heavier than hydrogen and helium. Thus, a low abundance of elements heavier than hydrogen and helium, such as iron, observed in a star indicates a very early formation time. It is these stars that are of greatest value for stellar archaeology and dwarf galaxy archaeology, because they provide a remarkably powerful tool for investigating the physical and chemical conditions of the early Universe. For example, the oldest stars enable us to isolate clean signatures from various nucleosynthesis processes that occurred prior to their formation. In this way, they uniquely contribute to nuclear astrophysics by providing information about elements that cannot be made or studied with nuclear physics experiments. From an astrophysics standpoint, these aspects of nuclear astrophysics explain how chemical enrichment proceeded in the cosmos, how the content of elements evolved with time, and how the presence of elements influenced early star and galaxy formation. In addition, studying these old stars enables one to connect the present state of the Galaxy with its long assembly history involving the accretion of neighboring smaller galaxies. These efforts are part of near-field cosmology, which aims to interpret the chemical abundances of the oldest stars from a broader, cosmological perspective.

In this context, I briefly review the structure and stellar populations of the Galaxy (**Figure 1**) (3). The Milky Way is a spiral disk galaxy containing a few hundred billion stars. It has a total dark matter mass of $(1.3\pm0.3)\times10^{12}~M_{\odot}$ and a total stellar mass of $(5\pm1)\times10^{10}~M_{\odot}$. The Milky Way and Andromeda, its slightly more massive sister galaxy, are by far the most massive galaxies in the Local Group. They are surrounded by approximately 50 known much smaller dwarf galaxies (with dark matter masses of $10^6-10^{10}~M_{\odot}$). The Galactic disk, which has a radius of 10-15~kpc, consists of several components: a thin disk with a vertical scale height of $300\pm50~pc$, a thick disk with a scale height of $900\pm180~pc$, and an even more vertically extended so-called metal-weak thick disk. The central $\sim3~kpc$ region of the Galaxy, the somewhat X-shaped bulge, is a very dense and luminous region of ongoing star formation that surrounds the Milky Way's central supermassive black hole of $(4.2\pm0.2)\times10^6~M_{\odot}$. Both the disk and, especially, the bulge are old structures, but

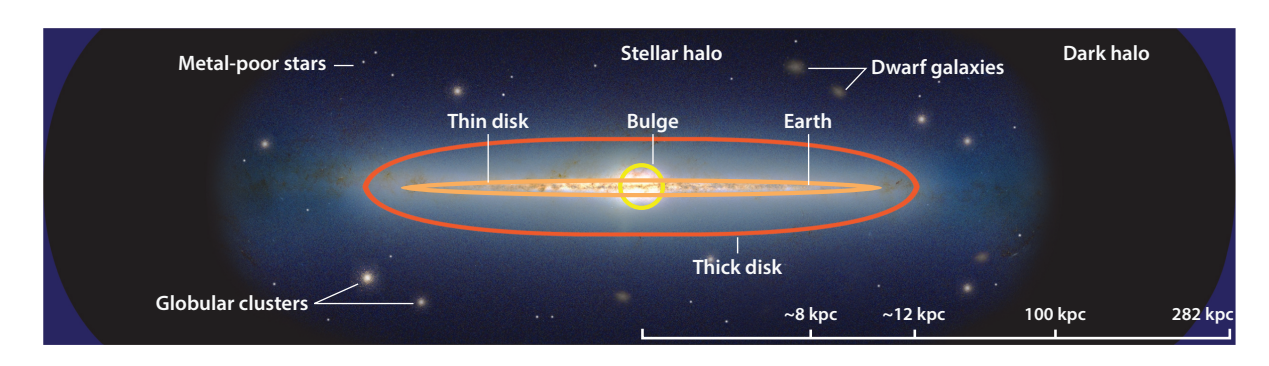


Figure 1

Structure and stellar populations of the Milky Way. Stellar archaeology is based on old, metal-poor halo stars. Dwarf galaxy archaeology utilizes stars in satellite dwarf galaxies that orbit the Milky Way. Figure adapted from image by K. Brauer.

they contain predominantly younger stars with near-solar abundances, although the bulge might contain a small number of the oldest stars left over from the Milky Way's earliest formation phase. For reference, the Solar System is located 8.2 ± 0.1 kpc from the Galactic Center. The disk(s) and bulge are enveloped by the so-called stellar halo, which is of much lower stellar density, and likely extends well beyond 100 kpc, where the farthest known stars are currently found. Also, the virial radius that includes the dark matter halo of the Galaxy is 280 ± 30 kpc. The stellar halo with $(4-7) \times 10^8$ M $_{\odot}$ hosts primarily older stars, globular star clusters, and those satellite dwarf galaxies that orbit the Milky Way. Debris and tidally ripped-apart dwarf galaxies form halo substructures with a combined $(2-3) \times 10^8$ M $_{\odot}$ and are responsible for extended star streams that span across the sky. Examples include the Sagittarius Stream, which originates in the Sagittarius dwarf galaxy and has left stellar debris throughout the halo, and the Monoceros Stream, which wraps twice around the Galaxy near the disk plane.

Stellar streams demonstrate how stars from dwarf galaxies can become mixed into the Milky Way. Once they are in the halo and several billion years have passed, it is (nearly) impossible to correctly assess their origin outside of the Galaxy. The same holds true for the oldest halo stars. They are likely older than the Milky Way itself and thus must have formed in some of the earliest star-forming galaxies, not unlike those dwarf galaxies that survived to orbit the Milky Way today. These early galaxies were later absorbed by the Galaxy as part of its own hierarchical growth, spilling all their stars into the stellar halo. The consequence is that, when we identify and work with these stars, we can only speculate about their origins and birth environments. This highlights the power of searching for old stars in satellite dwarf galaxies. These stars are still located within their natal system, which affords us the opportunity to assess their environment to draw firm conclusions about element-production events, how elemental yields were dispersed through the galaxy, and how the yields were eventually incorporated into the dwarf galaxy stars we observe. Studying stars and stellar populations in the satellite dwarf galaxies therefore provides an excellent complementary approach to working with halo stars. As discussed in in Section 4.1, research based on the composition of individual stars in dwarf galaxies recently led to a breakthrough in understanding the astrophysical site of the heaviest elements.

1.2. Review Aims and Further Reading

This review provides a compact overview of recent progress in understanding the origin and early evolution of the heavy elements that are made during the rapid neutron-capture process (*r*-process), as told by an astronomer. The goal of this review is to highlight links between what is studied by nuclear physicists (nuclear properties of matter) and what astronomers observe (stars with chemical abundance signatures that are the end result of various nucleosynthesis processes). New experimental nuclear physics facilities, such as the Facility for Rare Isotope Beams (FRIB), will investigate neutron-rich nuclei far away from stability, promising to yield an improved understanding of heavy-element production. Observations of the oldest stars in the Milky Way and its satellite dwarf galaxies provide complementary insights. They preserve a fossil nucleosynthesis record of astrophysical events of element production, providing valuable details concerning the nucleosynthesis processes involved and their associated astrophysical sites of operation.

This article's focus on neutron-capture elements means that, unfortunately, much of the related information on old stars, stellar archaeology, dwarf galaxy archaeology, near-field cosmology, and even nuclear astrophysics cannot be covered. Instead, I refer the interested reader to the following reviews:

■ a detailed overview of near-field cosmology, stellar archaeology, and dwarf galaxy archaeology with the oldest stars (4), and additional introductory material on the subject (5);

- a review of early progress, including the history of the search for old stars in the Galaxy (6);
- reviews on observations of neutron-capture elements in old stars and their interpretation (7, 8);
- reviews on neutron star mergers and associated heavy-element production (9, 10); and
- reviews on understanding the Galaxy in a cosmological context (3) and its formation when interpreting the chemical abundances of old stars (11).

2. CHEMICAL ABUNDANCE MEASUREMENTS OF OLD METAL-POOR STARS

I first summarize some of the technical details associated with the spectroscopic analysis of old stars that is required in order to extract their chemical element signatures. Typically, one interprets these signatures by comparing them with theoretical predictions of the elemental yields of various nucleosynthesis processes and/or astrophysical sources and sites. I then describe the characteristics of the chemically most primitive stars, namely the most iron-poor stars, to show how stellar abundances are used to learn about the nature and properties of the first stars.

2.1. Astronomy Jargon and Classifications of Metal-Poor Stars

In astronomy, the term "metals" collectively refers to all elements heavier than hydrogen and helium. Most stars are made from roughly 71% hydrogen, 27% helium, and up to a few percent of metals (i.e., all the other elements combined). However, the amount of metals in a star, also called metallicity, also depends on the star's formation time and birthplace. After the Big Bang, the Universe consisted of only hydrogen (75%), helium (25%), and trace amounts of lithium. The very first stars that emerged a few hundred million years later had masses of order $100 {\rm M}_{\odot}$ (12), likely ranging from ~10 to several hundred solar masses. Metal-free gas lacks sufficient coolants in the form of metals and/or dust grains that radiate away the thermal energy necessary for the gas to readily undergo gravitational collapse. Basic star formation models thus predict the formation of exclusively massive and short-lived stars, whereas stars with subsolar masses can form only once metals in the gas lead to more efficient fragmentation. Metals were indeed forged in the hot cores of the first stars in a series of fusion processes, leading to elements up to and including iron. Upon the explosion of these stars, the newly created material was dispersed into space, enriching the surrounding gas from which the next generation of stars formed. This process implies that the chemical evolution is the successive buildup of metals with cosmic time (Figure 2). It began with the element enrichments by the first exploding stars, and has progressed to a state where stars that are currently forming contain 2-4% metals (13). Consequently, stars that formed before the Sun was born 4.6 billion years ago generally have a lower metal content. Since the Sun is used as a reference, these older stars are called metal poor (compared with the Sun). Stars similar to the Sun (i.e., most stars) are referred to as metal rich. A handful of known stars are so metal poor that they are believed to be members of the second generation of stars (i.e., the first long-lived low-mass stars) to have formed after the Big Bang. The amount of metals they contain is so small that all heavy elements present in those stars could have been produced by a single progenitor star—one of the very first stars. For reference, the Sun formed from a gas cloud that was enriched by many nucleosynthesis processes and sites over the course of approximately nine billion years. The difference with respect to second-generation stars would be the equivalent of order 1,000 subsequently exploding massive stars enriching only the local gas. In reality, the process of chemical enrichment of a certain region is, of course, more complex and requires detailed modeling of all associated chemical, dynamical, and other evolutionary processes.

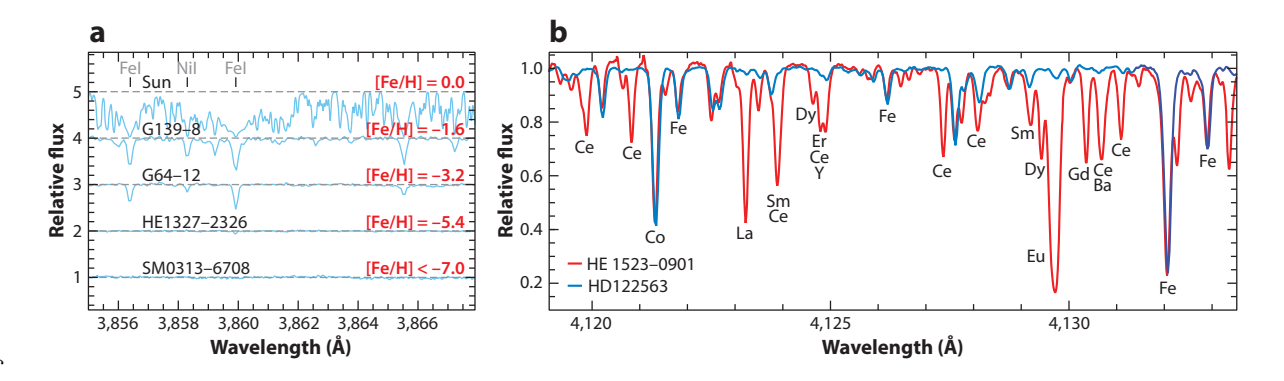


Figure 2
(a) Spectral comparison of stars with different metallicities, as shown by decreasing line strengths. In the bottom star, no iron lines are detected (14). Several absorption lines are marked. (b) Spectral comparison around the Eu II line at 412.9 nm of the r-process-deficient star HD122563 and the r-process-enhanced star HE 1523–0901. Both stars have similar temperatures and metallicities. Panel b adapted from Reference 15.

To describe the amount of metals in a star (i.e., its metallicity), one usually takes the abundance of iron as a proxy. This is part convenience, part necessity. It is not possible to determine the abundances of all elements from stellar spectra and add them up to obtain the total metal content. Instead, iron has numerous spectral absorption lines, and is thus relatively easy to measure. The chemical abundances of any two elements are then defined relative to the respective abundances in the Sun as $[A/B] = \log(N_A/N_B) - \log(N_A/N_B)_{\odot}$, where N_A (N_B) is the number of atoms of element A (B). By definition, the Sun has a metallicity of [Fe/H] = 0.0. An extremely metal-poor star would have [Fe/H] = -3.0, which corresponds to 1/1,000 of the solar iron abundance. Super-metal-rich stars have positive [Fe/H] values. Accordingly, the iron abundances are often thought to indicate a rough formation time, even though little is known about the complex age-metallicity relation (16). Stars with vastly different metal content have been discovered to date, spanning a total of at least eight orders of magnitude, from $[Fe/H] \sim +0.7$ to [Fe/H] < -7.3 (Figure 2) (14, 17). In the latter case, the iron abundance is so low that only an upper limit could be determined.

Numerous studies in the past three decades have validated that the iron abundance is indeed a good proxy for the overall metal content of a star. However, at the lowest metallicities, specifically [Fe/H] < -3.5, this fortuitous relation breaks down. A significant fraction of the stars show, for example, large enhancements of carbon over iron compared with the Sun (4), significantly increasing the total metallicity relative to just the iron abundance. Thus, it is important to refer to those stars as the most iron-poor instead of the most metal-poor.

To easily differentiate various classes of low-metallicity stars, Beers & Christlieb (22) introduced categories that classify the stars' metallicity and chemical signatures. **Table 1** presents an updated version of this list. The table first lists stellar-population classifications that are primarily of a historic nature but are still widely used. Next are the different metallicity classes, now extended to [Fe/H] < -10.0, following suggestions by T. Beers and I. Roederer (personal communications), followed by the stellar chemical signatures associated with enhancements in neutron-capture elements (i.e., those elements heavier than iron). The abundance criteria listed offer a quick classification; matching many more elemental abundances with the respective full patterns will confirm the nature of the star. **Figure 2** shows spectra of a regular metal-poor halo star and one enriched in heavy r-process elements.

The most significant change from the original classifications is the addition to **Table 1** of intermediate neutron-capture process (*i*-process)-enhanced stars, which are further discussed in

Table 1 Classes and signatures of metal-poor stars^a

Description	Definition	Abbreviation
Population III stars	Postulated first stars, formed from metal-free gas	Pop III
Population II stars	Old (halo) stars formed from low-metallicity gas	Pop II
Population I stars	Young (disk) metal-rich stars	Pop I
Super-metal-rich	[Fe/H] > 0.0	MR
Solar	[Fe/H] = 0.0	None
Metal-poor	[Fe/H] < -1.0	MP
Very metal-poor	[Fe/H] < -2.0	VMP
Extremely metal-poor	[Fe/H] < -3.0	EMP
Ultra-metal-poor	[Fe/H] < -4.0	UMP
Hyper-metal-poor	[Fe/H] < -5.0	HMP
Mega-metal-poor	[Fe/H] < -6.0	MMP
Septa-metal-poor	[Fe/H] < -7.0	SMP
Octa-metal-poor	[Fe/H] < -8.0	OMP
Giga-metal-poor	[Fe/H] < -9.0	GMP
Ridiculously metal-poor	[Fe/H] < -10.0	RMP
Signature	Metal-poor stars with neutron-capture element patterns	Abbreviation
Main r-process	$0.3 \le [Eu/Fe] \le +1.0 \text{ and } [Ba/Eu] < 0.0$	r-I
	[Eu/Fe] > +1.0 and $[Ba/Eu] < 0.0$	r-II
Limited r-process ^b	[Eu/Fe] < 0.3, [Sr/Ba] > 0.5, and [Sr/Eu] > 0.0	$r_{ m lim}$
s-process	[Ba/Fe] > +1.0, [Ba/Eu] > +0.5, [Ba/Pb] > -1.5	S
r- and s-processes	$0.0 < [Ba/Eu] < +0.5 \text{ and } -1.0 < [Ba/Pb] < -0.5^{c}$	r+s
<i>i</i> -process	$0.0 < \mathrm{[La/Eu]} < 0.6$ and $\mathrm{[Hf/Ir]} \sim 1.0^d$	i
Signature	Metal-poor stars with other element characteristics	Abbreviation
Neutron-capture normal	[Ba/Fe] < 0	No
Carbon enhancement	$[C/Fe] > +0.7 \text{ for } \log(L/L_{\odot}) \le 2.3$	CEMPe
	$[C/Fe] \ge [+3.0 - \log(L/L_{\odot})] \text{ for } \log(L/L_{\odot}) > 2.3^{f}$	CEMP
lpha-element enhancement	[Mg, Si, Ca, Ti/Fe] $\sim +0.4$	α-enhanced

^aThe table represents an updated version of the list in Reference 22, with some modifications and additions from Reference 5.

Section 3.2. Other neutron-capture-rich signatures are discussed in Sections 3.1 and 3.4, followed by the definition of carbon-enhanced metal-poor (CEMP) stars (23). More information on this prominent group of metal-poor stars can be found elsewhere (21, 23, 24). For completeness, I also include the commonly used criterion for α -element enhancement.

2.2. Element Abundance Analysis Techniques

The main goal of stellar spectroscopy is usually to measure the detailed chemical composition of the star (another reason is to obtain a star's radial velocity for kinematic analyses). This technique,

^bAlso referred to as the light-element primary process (LEPP) (18) or "weak" r-process.

^cBased on only one known carbon-enhanced metal-poor (CEMP)-r + s star (19); may require future adjustments.

^dMay require future adjustments (F. Herwig, personal communication).

eThe CEMP star definitions are from Reference 20. s- and i-process-enhanced stars are always CEMP stars; r-process-enhanced stars may or may not be CEMP stars. There is also a class of CEMP-no stars.

^fCarbon corrections as a function of luminosity can also be obtained from Reference 21.

and the telescopes used, is described in detail elsewhere (4, 5). Here, I summarize only key points for completeness. A high-resolution spectrum (with resolving power $R = \lambda/\Delta\lambda > 20,000$) covering visible wavelengths, ideally from ~ 350 to ~ 700 nm, is best suited for a detailed elemental abundance analysis, although spectra with low and medium resolution (1,000 < R < 6,000) also deliver abundances of a few key elements. Spectra obtained as part of large surveys (e.g., SDSS) often have low resolution. Examples of spectra at different resolution can be found in Reference 5. Near-IR spectra can be used to obtain a number of elements, as demonstrated in the APOGEE survey (25). Near-UV spectra are of considerable interest as well, especially for obtaining abundances of heavy neutron-capture elements with transitions only found there. However, such spectra are notoriously difficult to obtain (at present) for all but the very brightest stars (12 < V < 9), both because the stars of interest have low UV flux and because the mirror size of the *Hubble Space Telescope* is only 2.4 m.

Elemental abundances are obtained from the measured strengths of the spectral absorption lines of neutral and singly ionized species in the outer stellar atmospheres. This implies that abundances will be surface abundances but will still reflect the overall stellar abundances well, because of the unevolved nature and simple structure of the stars considered here. The abundances can then be calculated from the line strengths by use of a model atmosphere that approximates the physical conditions in the outer layers of the star, where the absorption occurs. One more component is required, namely the so-called stellar parameters, which consist of effective temperature ($T_{\rm eff}$), surface gravity (log g), chemical composition ([Fe/H]), and microturbulence ($v_{\rm mic}$). These parameters describe the atmosphere of a given star reasonably well, facilitating the choice of a model atmosphere to ultimately obtain the elemental abundances. Alternatively, synthetic spectra of known abundances can be computed and compared with the observed spectrum, as is often done in the case of molecular bands, or complex and blended absorption features, as is the case for many lines of neutron-capture elements. For a detailed discussion of how to determine stellar parameters and chemical abundances using various techniques, see Reference 5.

Note that the vast majority of stellar abundances are derived using simplified one-dimensional (1D) model atmospheres that assume local thermodynamic equilibrium (LTE) for the formation of all absorption lines in the outer stellar atmosphere. Considerable effort is ongoing to change this to a framework based on nonlocal thermodynamic equilibrium (NLTE) assumptions and threedimensional (3D) hydrodynamical modeling (26–28). Recent progress using quantum-mechanical atomic inputs for hydrogen collisions to determine stellar iron abundances under NLTE conditions is described elsewhere (29). This improvement is particularly relevant, since NLTE effects alter abundances derived from numerous and commonly used Fe I lines much more significantly than those derived from Fe II lines (30–33). With positive corrections, the metallicity of the stars increases, and the stars become more metal rich: only 0.25 dex for extremely metal-poor stars with $[Fe/H] \sim -3.0$ (compared with typical iron uncertainties of 0.1–0.2 dex) but 0.7 dex for the most iron-poor stars with [Fe/H] ~ -6.0 (which is significantly higher than any observational uncertainty). Computationally intensive 3D LTE (and even some 3D NLTE) stellar model atmospheres remain difficult to use for large samples of stars. Recent research has also shown significant abundance changes, especially for the most metal-poor stars and for elements derived from molecular species, such as CH (34, 35)

Despite these challenges, abundances of the light fusion elements up to and including iron are available (36) for more than 1,000 metal-poor stars. The most iron-poor stars (37–39) are the easily accessible local equivalent of the high-redshift Universe because they probe the very first chemical enrichment events that set in motion the chemical evolution. Therefore, these stars are used to reconstruct the properties of Population III stars (i.e., the first stars), their supernova explosions, and the associated nucleosynthesis processes. In this way, early metal and gas mixing

processes and assembly processes of galaxies can be constrained, aiding theoretical research on key questions related to the emergence of the first stars and galaxies from the primordial Universe, and helping to explain how the chemical elements produced in stars and supernova explosions were recycled through galaxies and eventually into planets and life. I refer the reader to Reference 4 for an in-depth discussion of the role of these lighter elements and the latest results.

3. SIGNATURES OF NEUTRON-CAPTURE ELEMENTS IN METAL-POOR HALO STARS

With the exception of hydrogen and helium, elements up to and including zinc (with atomic number $Z \leq 30$) are created through fusion processes in the hot cores of stars during stellar evolution and/or in explosive processes during supernova explosions if the stars were massive enough to explode (i.e., $M > 8 \, \mathrm{M}_{\odot}$). The remaining heavier elements are built up in neutron-capture processes, when the astrophysical environment provides seed nuclei (e.g., iron) and a certain flux of free neutrons. During rapid neutron capture (i.e., the r-process), the neutron-capture rate exceeds that of β decay, and large numbers of neutrons can be captured in 1–2 s, resulting in heavy neutron-rich nuclei that then decay back to stability to form the heaviest elements in the periodic table, ranging from strontium (Z = 38) to uranium (Z = 92). Approximately half of all stable isotopes of elements heavier than zinc are synthesized in this way (7, 40). The other half of the isotopes build up over much longer timescales, from the slow neutron-capture process (s-process), in which the capture rate is lower than the β decay rate of the unstable isotopes. The postulated intermediate neutron-capture process (i-process) is somewhat similar to the s-process but requires significantly higher neutron densities. In the following subsections, I describe the s-, i-, and r-processes, and highlight discoveries of metal-poor stars with their respective elemental signatures.

3.1. The Astrophysical Signature of the s-Process

Neutron-capture element production through the s-process occurs in stars with $1-8~M_{\odot}$ during the last $\sim 1\%$ of their lifetime. Stars with $1~M_{\odot}$ live for 10 billion years, whereas stars with $8~M_{\odot}$ shine for just under 100 million years. Their last evolutionary stage is the so-called asymptotic giant branch (AGB) phase, during which such stars are thermally pulsating. In the AGB phase, a star has an inert carbon–oxygen core surrounded by the helium-burning shell, followed by a helium-rich intershell region and a hydrogen-burning shell. Farther out is the convective envelope that reaches to the surface (see Reference 41 and references therein). These stars ultimately end their lives as regular stars and become so-called planetary nebulae. Thereafter, the outer gas layers are expelled to expose the hot core, a so-called white dwarf made from either carbon and oxygen or oxygen, neon, and magnesium. I now describe how the s-process operates in stars with specific stellar masses, as they produce elements with different atomic masses.

3.1.1. The main s-process. The dominant neutron source (leading to a neutron density of $n_n \sim 10^8$ cm⁻³) in low-mass stars with 1–3 M_{\odot} is the 13 C(α ,n) 16 O reaction (42). However, this reaction can occur only if sufficient protons are mixed from the hydrogen-rich shell down into the helium intershell. Then, the so-called 13 C pocket is activated, because the protons can combine with existing 12 C to form 13 C (through partial completion of the CN cycle) and produce neutrons. This series of processes eventually enables neutron capture onto seed nuclei, such as iron, to create s-process elements. Although many details relating to the existence and operation of the proton-mixing episodes and buildup of the 13 C pocket remain under debate (see Reference 41 for a review), the s-process only operates with it in place (43–46). This process is called the main

s-process because it provides a substantial neutron exposure (the time-integrated neutron density) that leads to the formation of elements with Z > 40 in the second and third s-process peaks, in between the convective thermal pulses, on timescales of 1,000 to 10,000 years. During each pulse, these newly created elements, as well as copious amounts of carbon, are dredged up to the stellar surface and are eventually released into the surrounding interstellar gas through stellar winds. Given the large number of these stars (lower-mass stars are more common than higher-mass stars), this stellar population contributes significantly to the inventory of neutron-capture elements, as well as carbon, in the Universe.

Indeed, the overall emergence of s-process material in star-forming gas is documented by the body of observations of metal-poor halo stars with metallicities of [Fe/H] > -2.6 that formed as part of the next stellar generation following the initiation of substantial s-process enrichment. Note that at lower metallicities, insufficient seed nuclei, such as iron, are available for the s-process to operate, although earlier, individual contributions of s-process elements by short-lived massive stars are likely (47). Stars at various metallicities thus reflect consistently increasing enhancements in s-process elements, such as barium, but also increasing amounts of other lighter (fusion) elements, as part of ongoing chemical evolution.

This evolution highlights a central challenge for stellar archaeology. While many metal-poor stars clearly show signs of the s-process operating (e.g., enhanced barium abundances), because of their already-higher [Fe/H] values it is not possible for us to discern how many progenitor stars contributed s-process nuclei to the local gas prior to when these stars formed. Thus, a clean signature of only one prior s-process cannot be reliably obtained from ordinary metal-poor stars with [Fe/H] > -2.6. Fortunately, there is another way. Around 10% of these metal-poor stars show extreme enhancements in s-process elements. An additional few such stars are found in dwarf galaxies (48). These low-mass stars happen to be part of binary star systems, each with a companion star that is slightly more massive and thus more evolved (less-massive stars live longer than moremassive stars). The erstwhile companion is thought to have undergone the AGB phase, produced copious amounts of s-process elements (and carbon), and then transferred the enriched surface material to the now-observed star, where the transferred mass dominates the surface composition. Such mass-transfer events are common in binary systems of stars with orbital separations that are sufficiently small to experience Roche lobe overflow after one star (the more massive of the pair) inflates during late stellar evolution. This scenario has been confirmed by long-term monitoring of the radial velocities of such stars. Velocity variations are found in 80% of them (49) due to the observed star's motion around the (now usually unseen) companion. Naturally, large amounts of carbon are also transferred. What is then observed in these metal-poor stars is the characteristic signature of the main s-process element, together with carbon enhancement, which is the result of only one progenitor: the companion star (50, 51).

The signature of the main *s*-process can be easily recognized from the three telltale peaks in the abundance distribution, as a function of atomic number Z (7, 52). The first peak is located at Z = 38–40 (strontium, yttrium, zirconium), the second at Z = 56–60 (barium through neodymium), and the third at Z = 82–83 (lead and bismuth, the termination point of the *s*-process, as shown in **Figure 3**). Assuming sufficient neutron exposure, the peaks are the result of certain nuclei having low cross sections, and thus being particularly stable against neutron capture. This occurs for nuclei with a magic number of neutrons, namely 50, 82, or 126. Nuclei that also have a magic number of protons are the most stable; these include ²⁰⁸Pb with 126 neutrons and 82 protons. These nuclei become bottlenecks during *s*-process nucleosynthesis and lead to the characteristic *s*-process peaks. At very low metallicity (e.g., $[Fe/H] \lesssim -2.0$), the observed nucleosynthesis pattern shows exactly this abundance distribution, including extreme lead abundances (56–58), due to the increased neutron exposure, as the *s*-process operates with a comparatively large

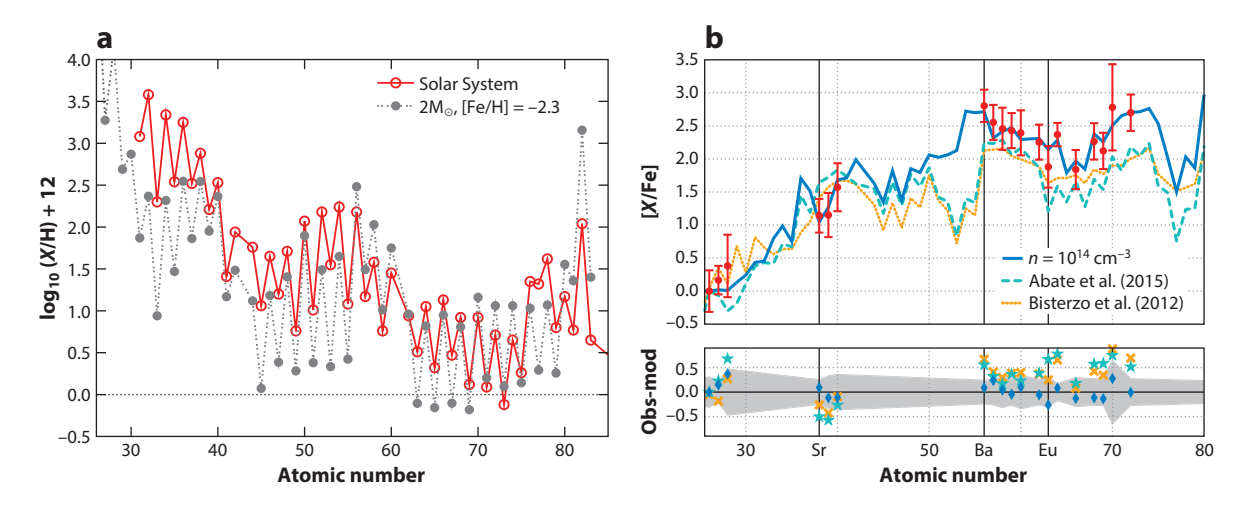


Figure 3

(a) The s-process (absolute) abundance pattern inferred for the Sun compared with that calculated to be produced by a 2 M_{\odot} evolved star with [Fe/H] = -2.3 (45). At low metallicity, the s-process operates efficiently enough to produce s-process abundances equal to or greater than the Solar System values, including large amounts of lead (Z=82). (b) Abundances (red circles) of the star LP 625–44, overlaid with nucleosynthesis models of the s-process (cyan) (53), s-process plus an initial r-process enhancement (orange) (54), and the i-process (blue) (55). Residuals of models and data are shown at the bottom. The gray area reflects observational uncertainties from the top panel. Panel a adapted from image by A. Karakas. Panel b adapted from image by M. Hampel.

neutron-to-seed ratio arising from the sparsity of, for instance, iron atoms. Then, the *s*-process completes because there is no lack of neutrons—that is, all the way up to lead. Predictions for the yields of low-metallicity *s*-process models are able to broadly reproduce the observed patterns, including the high lead abundance (59).

Somewhat different s-process patterns are produced in stars with progressively higher metallicity. This metallicity dependence of the s-process, as well as the fact that at least two different sites host s-process nucleosynthesis (see Section 3.1.2), implies that this process is not universal but rather environment dependent. More metal-rich stars produce s-process signatures with much lower lead abundances. If cleanly observed, such as in a binary companion star, those patterns match the (slightly scaled) solar pattern. Note that considering the total solar abundances at face value does not tell us how much of each element (or each isotope) was made in the s-process, or the r-process, over the course of the nine billion years prior to the Sun's formation. In order to obtain the solar s-process pattern, it has to be calculated. Given that s-process nucleosynthesis occurs along the valley of β stability, neutron-capture rates and other nuclear properties have been successfully studied with experiments (in contrast to the r-process, which occurs far from stability; see Section 3.4). Consequently, the s-process is theoretically well understood (52, 60), and the solar s-process component (or pattern) has been calculated, taking into account Galactic chemical evolution as well (19, 46, 61).

3.1.2. The weak *s*-process. In stars with intermediate masses of 3–8 M_{\odot} , the reaction $^{22}\mathrm{Ne}(\alpha,n)^{25}\mathrm{Mg}$ serves as the dominant neutron source (42). It follows $^{14}\mathrm{N}(\alpha,\gamma)^{18}\mathrm{F}(e^+ + \nu)^{18}\mathrm{O}(\alpha,\gamma)^{22}\mathrm{Ne}$, based on initial $^{14}\mathrm{N}$ stemming from the CNO cycle. It operates during the thermal pulses within the helium intershell on timescales of 10 years. The resulting neutron density is significantly higher than what is produced in low-mass stars, $n_n > 10^{10}$ cm⁻³ (41, 62), but the neutron exposure is reduced (due to the shorter timescale). The resulting *s*-process is called

the weak s-process, and produces elements in the region of the first s-process peak, around $Z \sim 40$ (52). This neutron source also operates during core helium and shell carbon burning in massive stars with >12 M_{\odot} that eventually explode as supernovae. It produces an s-process-element distribution similar to that of intermediate-mass AGB stars (63). Finally, it has also been suggested to operate in massive, rotating ($\sim 500-800 \text{ km s}^{-1}$ at the equator), near-metal-free stars (64, 65). Fast rotation boosts s-process-element production by several orders of magnitude [e.g., for strontium (see Reference 47 and references therein)] because rotation-induced mixing increases the production of ¹⁴N, ¹³C, and ²²Ne, all of which aid in the operation of the s-process. The yields provide qualitative explanations for unusual abundance patterns [e.g., [Sr/Fe] = +1.2 in HE 1327–2326 with [Fe/H] = -5.4 (37)] and subsolar [Sr/Ba] ratios in some metal-poor stars. However, more theoretical research may be needed to further refine predictions.

3.2. The Astrophysical Signature of the *i*-Process

Some 20 CEMP stars are known with distinct neutron-capture-element signatures that match neither the pattern of the s-process nor that of the r-process. Therefore, they were originally classified as CEMP-r/s stars (6). For more than a decade, there has been extensive speculation as to whether a combination of the two processes might explain the observations. This group of objects became known as the CEMP-r + s or CEMP-s + r stars. However, no unambiguous explanation could be found (66–69). Instead, given these stars' resemblance to s-process-enhanced stars with large carbon abundances, recent theoretical research has begun to suggest that a neutron source intermediate between the s- and r-processes might be operating, and responsible for these observed chemical signatures. This led to the (re)introduction of the so-called intermediate neutron-capture process, or *i*-process (55, 70), following an original suggestion by Cowan & Rose (71). This process supposedly operates under neutron densities of $n_n \approx 10^{15} \, \mathrm{cm}^{-3}$, several orders of magnitude higher than what is required for the s-process $(n_n \sim 10^8 \, \mathrm{cm}^{-3})$; see Section 3.1), but likely varying neutron exposures (70). Invoking a large neutron exposure (52) results in an increased production of heavy neutron-capture elements at and above the second peak (roughly 55 < Z < 75), as is needed to match the observations. Abundances of metal-poor stars with the CEMP-r/s (or suggested CEMP-r + s or similar) label can be well reproduced with nucleosynthesis calculations using neutron densities of $n_n \sim 10^{14}$ cm⁻³ (55). By contrast, observations of mainly first-peak elements in some post-AGB stars point to low neutron exposure (72). However, if the *i*-process is truncated before reaching equilibrium, it can stop producing elements at almost any atomic number, thereby producing few or even no neutron-capture elements (73).

The astrophysical site(s) of this process remains in question. The best candidates are low-to intermediate-mass, low-metallicity AGB stars. They could potentially produce a significant burst of neutrons over sufficiently long timescales within the convective helium intershell region, if the necessary numbers of protons enter this region from above the hydrogen-burning shell (74). Alternatively, in the most massive "super-AGB" stars (75), the protons could enter during a core helium flash (76, 77). Yet another possibility involves rapidly accreting white dwarfs in close binary systems (78). These protons could then combine with the available 12 C to form 13 C, so that the 13 C(α ,n) 16 O reaction can produce a sufficiently high neutron density [up to $n_n \sim 10^{15}$ cm $^{-3}$ (79)] for the *i*-process to operate, similar to the *s*-process (see Section 3.1). The resulting nucleosynthesis yields would all arise from an environment with roughly similar neutron densities and independent of the proton ingestion mechanism (80). However, the neutron exposure would vary significantly with astrophysical site. The AGB stars would likely provide environments of high neutron exposure, whereas evolved massive stars would produce low exposure during hydrostatic helium and carbon burning (63).

Overall, ample observational data suggest that the *i*-process has contributed to the composition (see Reference 73 for a full list) in, for example, the post-AGB star known as Sakurai's object (72), in presolar grains (81), and in metal-poor stars with supersolar [As/Ge] and solar or subsolar [Se/As] ratios (73). More theoretical research is needed to ascertain the details of potential astrophysical sites, as well as yield predictions, to explain the full range of metal-poor stars with these unusual enhancements in neutron-capture elements.

3.3. Star with Signatures from Both the r- and s-Processes

Despite many attempts to explain the neutron-capture-element signatures of i-process-enhanced stars as a result of the combination of s- and r-process elements (66–69), and the overall plausibility of this scenario, it is surprising that no stars with such a signature have been discovered. However, recent searches for r-process-enhanced stars (82, 83) have finally delivered the first example. Gull et al. (19) describe a metal-poor giant star, RAVE J0949-1617, with [Fe/H] = -2.2 and carbon enhancement ([C/Fe] = 1.2), that displays a combination of enhanced s- and r-process elements. Note that the elemental signature of RAVE J0949-1617 is unlike that of the i-process when compared with model predictions (55). The likely scenario for a star such as RAVE J0949-1617 is that it must have formed in a binary system from gas enriched by a prior r-process event and, later on, received carbon and s-process material during a mass-transfer event from the binary companion star. A combination of isotopes made in the two processes is now observed in the form of an unusual neutron-capture-element pattern that is governed by high barium and lead abundances (due to the s-process component) and lower rare-earth-element values (from the r-process). Figure 4 shows the abundance pattern of this star. Modeling the combination of the two processes, following Reference 53, revealed an initial r-process enrichment of 0.6 dex of the natal gas cloud, making the star a moderately r-process-enhanced star that happens to be in a binary system. While other

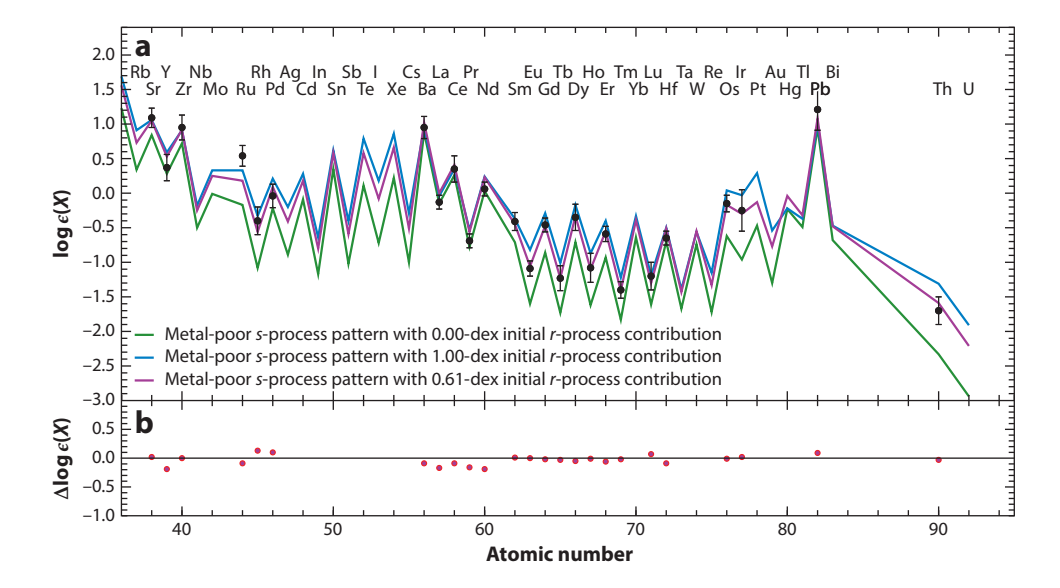


Figure 4

(a) Abundances (black circles) of star RAVE J0949–1617, overlaid with s-process yields to which different initial r-process enhancements have been added. (b) Residuals between the best-fit model and the observed

data. Adapted from Reference 19.

combinations of the amounts of r- and s-process elements are possible, more of these stars need to be discovered to assess whether any similarities to i-process-enhanced stars exist.

For now, it remains puzzling as to why no other bona fide CEMP-r+s stars have yet been found. The fraction of low-mass metal-poor stars in binary systems is ~16% (84); the fraction of moderately r-process-enhanced stars is ~15% (see Section 3.4). At face value, CEMP-r+s stars should therefore be rare, ~2%, but they are still only half as common as the rare highly r-process-enhanced stars, of which at least two dozen are known at present. Thus, more than one CEMP-r+s should have been found by now. This could suggest that the binary fraction was perhaps lower than previously thought, that some process prevents the proper identification of CEMP-r+s stars (19), or some other reason. While discovery of more of these stars is awaited from ongoing and future searches, for now this single object defines the class of bona fide CEMP-r+s stars.

3.4. The Astrophysical Signature of the r-Process

Rapid neutron capture occurs when the neutron density reaches $n_n > 10^{22}$ cm⁻³. Then, seed nuclei are bombarded with neutrons to form neutron-rich isotopes far from stability, including those in the transuranian region, within only 1–2 s. Once the neutron flux stops, the nuclei decay to form stable isotopes, including the actinide elements thorium (Z = 90) and uranium (Z = 92). The resulting abundance distribution is difficult to predict ad hoc, but abundance results for the Sun have shown a characteristic elemental pattern that is also found in metal-poor stars with enhancements in neutron-capture elements (7). This pattern is also described by three abundance peaks, but they are distinctly shifted to lower mass numbers, compared with the s-process pattern. The first peak occurs at Z = 34–36 (selenium, bromine, krypton), the second at Z = 52–54 (tellurium, iodine, xenon), and the third at Z = 76–78 (osmium, iridium, platinum). The peaks in the s-process distribution are due to the pileup of stable nuclei with magic neutron numbers (see Section 3.1). In the r-process, the peaks result from the decay of unstable neutron-rich nuclei with magic numbers of neutrons, leading to peaks at lower mass numbers than the s-process.

Only a few astrophysical sites can produce such high neutron densities. Candidate sites are thus limited to core-collapse supernovae, magnetorotationally jet-driven supernovae, and mergers of a binary neutron star pair or a neutron star–black hole pair (see Reference 10 and references therein). Identifying this site (or sites) has remained a major challenge for nuclear astrophysics since the 1950s, when researchers first recognized that the r-process is required to account for the solar abundances of heavy elements (85, 86). Recent astrophysics observations of old stars in a dwarf galaxy have finally shown neutron star mergers to be the most likely production site (87). This example of the interplay of astrophysics and nuclear physics to identify the site of the r-process is discussed in more detail in Section 4. Here, I provide a general description of the observational data on the r-process available through metal-poor stars, and refer the reader to Reference 7 for a discussion of the Sun's r-process pattern.

Ample evidence exists that the r-process operated in the early Universe, specifically in the form of rare metal-poor stars showing unusually large amounts of neutron-capture elements associated with the r-process in their spectra. Their corresponding elemental abundances exhibit the characteristic signature of the r-process; examples are shown in **Figure 2a**. Dedicated searches for these r-process-enhanced stars (88) found that they are quite rare: 3–5% of otherwise-ordinary metal-poor stars with [Fe/H] < -2.5 in the Galactic halo contain a strong enhancement of r-process elements (89). Recall that these stars did not produce any of these elements themselves. In fact, r-process enhancement is found across all major phases of stellar evolution (90), further indicating that these elements are not the result of any peculiar atmospheric chemistry. Based on long-term monitoring of their radial velocities (91), the great majority of r-process-enhanced

metal-poor stars (\sim 82%) exhibit no variations arising from the presence of a binary star companion. Thus, mass transfer from the companion to the presently observed star cannot be the cause of its r-process enhancement; rather, r-process-enhanced stars preserve the chemical fingerprint of the nucleosynthesis processes that enriched their birth gas clouds. These natal environments are expected to have been enriched by core-collapse supernovae in light elements (found in all metal-poor stars), as well as an r-process event that provided the neutron-capture elements observed. The low metallicity of the stars implies that r-process nucleosynthesis must have already taken place in the early Universe, in environments with limited additional star formation, so as not to erase the distinctive r-process patterns. Only one (or very few) progenitor supernova would be needed to produce the (small) amount of iron found in extremely metal-poor stars with $[Fe/H] \sim -3.0$.

As for the r-process elements, one can likewise assume, in a first instance, that only one progenitor event produced them. This makes these stars particularly interesting for stellar archaeology. However, stars that challenge this notion (those with the actinide boost; see Section 3.4.4, below) are also being found (92, 93). These cases might be due to the r-process operating in multiple sites, or variations of nucleosynthetic pathways within a given site. The question of progenitor objects and events is further complicated by suggestions that there may have been differences in the birth environments and in the associated levels of r-process yield dilution within the natal gas clouds from which these r-process-enhanced stars formed. This idea is supported by r-process-enhanced stars with higher [Fe/H] values. They may simply have formed in larger systems in which the r-process was diluted more, or from gas enriched by multiple progenitors objects and/or events.

The europium abundance relative to iron, [Eu/Fe], is commonly used to quantify the level of rprocess enhancement (**Table 1**). Two levels of r-process enrichment are (arbitrarily) distinguished for convenience. The strongly enhanced r-II stars have [Eu/Fe] > +1.0, whereas the moderately r-process-enhanced r-I stars show +0.3 < [Eu/Fe] < +1.0. The group of r-II stars thus exhibits europium-to-iron ratios more than 10 times that of the Sun, indicating that, compared with lighter elements such as iron (which determine the metallicity of the star), unusual amounts of r-process elements are present. Approximately 30 of them are currently known. Many more r-I stars, around 130, have been discovered to date, corresponding to ~15% of metal-poor stars. Examples of wellstudied r-II stars include the very first one to have been discovered, CS 22892-052 (94), which is also a carbon-enhanced star; the first star with a uranium measurement, CS 31082-001 (95), which also exhibits an actinide boost (see Section 3.4.4); and HE 1523-0901, which also has a uranium measurement (96). All three stars have [Fe/H] ~ -3.0 , but the neutron-capture material is 40-70 times more abundant relative to iron. Interestingly, the metallicity distribution of both r-I and r-II stars broadly covers the range $-3.5 < \text{[Fe/H]} \lesssim -1.5$. However, at [Fe/H] ~ -1.5 , the median [Eu/Fe] of halo stars is [Eu/Fe] $\sim +0.3$. This is where the classification of r-processenhanced stars ceases to be useful, since nearly 50% of halo stars have [Eu/Fe] > 0.3 and would thus be r-I stars. In these cases, only stars showing the r-process pattern can be identified as truly r-process-enhanced stars. Note that, in this context, metal-poor stars with [Fe/H] < -2.6naturally show neutron-capture-element signatures free of any s-process contribution, since the s-process begins to contribute significantly to the chemical enrichment of star-forming gas only around [Fe/H] ~ -2.6 (97). At [Fe/H] > -1.4, the r-process stops dominating the chemical evolution of neutron-capture elements (98).

I now describe three different groups of astrophysical conditions and sites that enable r-process nucleosynthesis (details are given in **Table 2**). This description of the underlying physics processes will help us understand different portions of the observed r-process abundance pattern that may arise from contributions from different astrophysical sites.

3.4.1. The early phase of any r-process: quasi-statistical equilibrium and the hot versus cold r-process. One form of the r-process, the so-called hot r-process, undergoes an initial quasi-statistical equilibrium (QSE) phase, which typically creates elements from strontium to silver, before significant neutron capture takes place (the case of a stand-alone terminal QSE is also possible under conditions that prevent any additional neutron capture to create elements heavier than silver). A hot r-process operates at $T > 10^9$ K, when hot and dense material initially consisting of protons and neutrons is expanding, such as in any kind of wind emerging from a supernova or neutron star merger environment. During the QSE phase, seed nuclei are created close to stability, from α , neutron, and proton captures and the reverse processes. Neutron capture onto these newly created seeds, such as strontium, eventually occurs during the subsequent r-process, but conditions are not suitably neutron rich to consistently produce elements heavier than silver.

In contrast, the cold r-process operates at $T\sim 10^8$ K. Neutrons become available when, for instance, (α,n) reactions are activated by shock heating in a supernova. Subsequent neutron capture takes place onto preexisting seeds, such as iron, in the birth material of the supernova progenitor. Due to the lower neutron density, the neutron-rich nuclei produced in this way are much closer to the valley of β stability compared with nuclei made in the hot r-process.

3.4.2. The main r-process. It has been well established that the observed abundances of r-process elements in r-process-enhanced stars display essentially the same relative pattern for elements barium and above, even though the absolute enhancement levels of these elements vary by \sim 1.5 orders of magnitude (as evidenced by, e.g., the range of europium and the associated iron abundances). **Figure 5** displays rare-earth elements with $56 \le Z \le 70$ in various r-process-enhanced stars. These abundance patterns show little scatter, in contrast to the lighter elements around $Z \sim 40$. Remarkably, the stellar r-process patterns are also nearly identical to the scaled solar r-process component (61) that can be extracted from the total solar abundances by subtracting

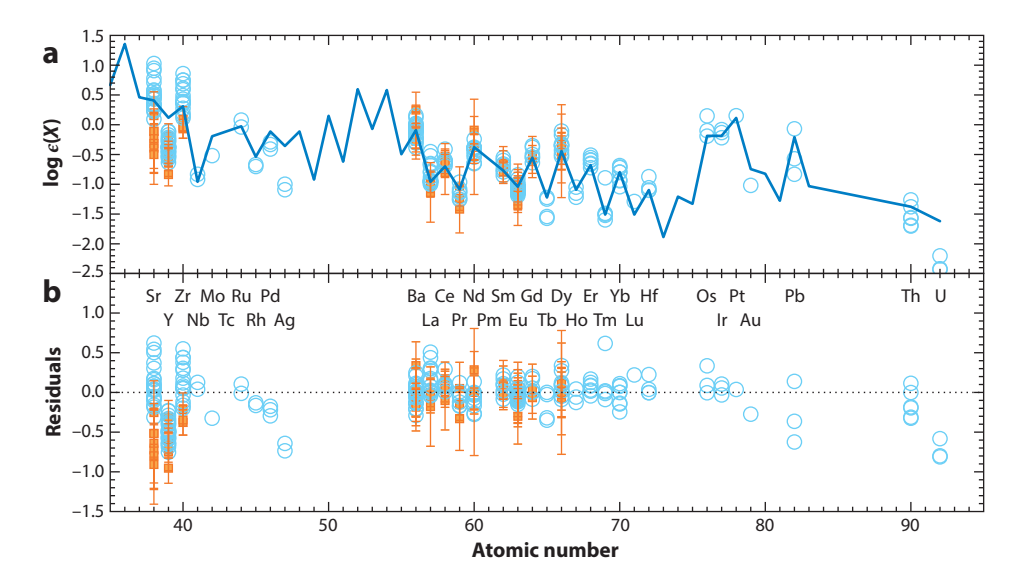


Figure 5

(a) Normalized r-process-element abundances of metal-poor halo (open circles) and Reticulum II stars (orange squares), overlaid with the scaled solar r-process pattern (line) (61). (b) Differences between the stellar abundances and the solar pattern. Adapted from Reference 142.

the theoretically calculated s-process component (see Section 3.1). Given that the Sun formed billions of years after these metal-poor stars, from gas that was enriched by many stellar generations in various ways, the astounding agreement between the patterns suggests that the r-process is universal, at least for elements in and above the second peak (99). No matter where and when the r-process occurs, the elemental signature appears to be robust. This is referred to as the main r-process. Elements with Z > 70 show somewhat more scatter, which is at least partially due to observational uncertainties. Thorium and uranium, of course, canonically differ from the scaled solar pattern due to their decay (with actinide-deficient/actinide boost stars as exceptions; see Section 3.4.4).

Note that even though measurements of isotope abundances would be very insightful for studying the universality of the main r-process, they are impossible to determine for most elements, for various reasons (100). The only exceptions are barium, europium, and possibly neodymium and samarium, but results are often too uncertain to actually provide stringent constraints on their (isotopic) formation process (101). In addition, it is astounding to recall that the r-pattern was discovered on the basis of the derivation of 1D LTE abundances, despite the range of metallicities covered by the stars. The stability and reproducibility of the pattern imply that systematic abundance uncertainties, such as NLTE or 3D effects, cannot be of a significant differential nature for ionized species in the rare-earth regime, although these heavy elements might still be equally affected (which would simply shift uniformly but not differentially change the pattern). The universality of the main r-process offers a unique opportunity to provide observational constraints on theoretical modeling of the r-process because the stars clearly suggest only one end result. This enormous advantage makes r-process-enhanced stars ideal test objects for nuclear physics, complementing nuclear physics experiments, which cannot yet reach the heaviest neutron-rich nuclei involved in the r-process.

But which site can produce this end result? Generally, a very neutron rich environment with an electron fraction of Y_{ϵ} < 0.2 is required to produce the second- and third-peak r-process elements. The electron fraction, $Y_e = 1/(1 + N_n/N_p)$, is the ratio of electrons to baryons (i.e., neutrons and protons) that describes the neutron richness and is a critical parameter that ultimately determines which elements are made (102, 103). It changes when protons capture electrons to form neutrons and, thus, with the environmental conditions where an r-process can occur. Accordingly, moderately neutron- or proton-rich QSE conditions with $Y_e \gtrsim 0.5$ (when $N_n/N_b < 1$) enable the synthesis of first-peak elements. The main r-process thus operates under $Y_e < 0.2$ conditions that become as extreme as $Y_e \sim 0.05$. In such a neutron-rich environment, with a neutron-toseed ratio of $\gg 100$, fission cycling occurs before the r-process freezes out. This fission cycling nuclei in the second-peak region are produced from the fission of neutron-rich nuclei in the transuranian region. The fission products then become seed nuclei themselves, contributing again to the formation of elements barium to uranium. Depending on the amount of fission cycling, the main r-process can be split into two components. A standard main r-process feeds on any amount of fission cycling, whereas a particularly robust main r-process runs at the fission cycling limit, that is, a constant fission-induced production of second-peak elements. Both of these r-processes create elements barium to uranium, and produce the kind of universal r-process patterns that are found among r-process-enhanced metal-poor stars and the Sun. Table 2 lists the various nucleosynthesis processes and conditions that produce certain element groups as part of what is generically called the r-process. Astrophysical sites where an r-process can operate are described below.

The astrophysical site now believed to be the prime candidate for hosting any type of main r-process is during the merger of a pair of orbiting neutron stars. Neutron stars are the compact remnants of stars with masses of $10-20~{\rm M}_{\odot}$. High-mass stars were likely dominant early on in the Universe, with a propensity to be born as binaries or multiples (105). Modeling of a main r-process occurring during the very complex merger process (consisting of different phases and components)

Table 2 Nucleosynthesis processes that can contribute neutron-capture elements

	I	I	1	
		Elements		
Process	Conditions	produced	Y_e	Astrophysical sites
Terminal QSE ^a	Insufficiently neutron rich; α , neutron, proton capture and reverse; expansion from hot, dense state	$Sr \rightarrow Ag$	<0.5	Standard proto-neutron star wind in core-collapse supernovae; shock-heated/disk ejecta
νp-process	Proton rich, $\overline{\nu}_e$ rich; QSE and $\overline{\nu}_e$ capture	$Sr \rightarrow Ag$	>0.5	Standard proto–neutron star wind in core-collapse supernovae; shock-heated/disk ejecta
Limited r-process ^b	Neutron-to-seed ratio ≪100; QSE and (limited) neutron capture; no fission cycling	$Sr \rightarrow Ba$ (limited production) toward Ba	<0.5	Modified proto-neutron star wind; neutron star merger: disk (after merger, viscous/wind timescales); shock-heated ejecta (during merger, dynamical timescales)
Main r-process	Neutron-to-seed ratio > 100; QSE and neutron capture; any fission cycling	Ba→ U	<0.2	Neutron star merger: tidal ejecta (during interaction); dynamical ejecta (during merger)
Robust (main) r-process	Neutron-to-seed ratio >100; QSE and neutron capture; fission cycling limit	$Ba \rightarrow U$	<0.2	Neutron star merger: tidal ejecta (during interaction); dynamical ejecta (during merger)

^aQuasi-statistical equilibrium; see Reference 104 for a detailed description and treatment.

has been extensive (see References 9, 10, and 106–108 and references therein) because conditions are generally very favorable, especially in the initially (cold) dynamical ejecta that occur during the merger phase (109). Since these ejecta all have $Y_e < 0.1$, only second- and third-peak elements with Z > 50 are made (110). The corresponding predicted high elemental yield of these ejecta is principally commensurate with the overabundances of heavy r-process elements found in r-II stars (87).

Additional r-process production occurs in the neutrino-rich winds emanating from the disk surrounding the merged object. These disk winds develop through a combination of viscous heating and nuclear heating following α particle formation, and might be able to eject more material than the dynamical ejecta (111). Weak interactions might significantly increase the Y_e of the disk material, which could result in the production of all three peaks of the r-process elements, but many parameters influence the eventual Y_e distribution. The observed nucleosynthetic signature of a neutron star merger is, in all likelihood, a combination of these two types of ejecta, with disk wind yields being less robust than those of the dynamical ejecta. The resulting, observable r-process signatures may show at least some scatter, in particular among first-peak elements. Halo star observations might thus be able to place stringent constraints on the Y_{ε} distribution of the progenitor r-process event and possibly even its components. This topic is discussed further below and in Section 4. For completeness, I note that a similar heavy-element pattern was predicted to be produced by magnetorotationally driven jet supernovae (112). However, new calculations cast doubt on the feasibility of this scenario (113) and on the previously obtained high r-process yield (similar to that of a neutron star merger), suggesting that these types of supernovae are not likely to be the main producers of r-process elements in the early Universe.

 $^{^{}b}$ Often referred to as the weak r-process or the light-element primary process (LEPP). However, the term "weak" does not well describe the nature of the underlying r-process physics, and "LEPP" does not refer to a specific nuclear physics process.

3.4.3. The limited r-process. While the r-process pattern appears to be universal for elements in and between the second and third peaks, deviations among first-peak elements and actinide elements from, for instance, the solar pattern are regularly observed in r-process-enhanced stars. Specifically, a few r-process-enhanced metal-poor stars display first-peak abundances higher than the solar pattern (when scaled to heavier elements such as europium), whereas most stars have lower values. **Figure 5** illustrates these relative first-peak deviations. In the case of strontium, they cover a significant 1.5-dex spread around the solar pattern. Reasons for these discrepancies remain unknown, but the observed spread has been interpreted as evidence for multiple r-processes or r-process sites (18, 92, 94, 114, 115). A kind of "failed" r-process would be able to produce only light neutron-capture elements with Z < 56, which led to the terms "weak r-process" (116) and "light-element primary process" (LEPP) (18). Instead, by focusing on the underlying conditions of the r-process, this type of nucleosynthesis should be referred to as the limited r-process due to a limited neutron-capture rate, as shown in **Table 2**.

From a theoretical point of view, the limited r-process begins with a phase of QSE. An insufficient neutron-to-seed ratio of \ll 100 then enables only limited neutron capture to take place, preventing the production of the heaviest elements. Consequently, only light neutron-capture elements around the first peak are made, with a rapidly decreasing production toward second-peak elements. Generally, this process might operate in (modified) neutrino-driven winds emerging from a proto–neutron star formed after a core-collapse supernova in a progenitor star of perhaps $8-10~{\rm M}_{\odot}$ (116, 117). Alternative sites are winds from the accretion disks that form after the merger of two neutron stars, or the shock-heated ejecta during such a merger. For completeness, I note here that the νp -process yields an element distribution very similar to that of the limited r-process. It plausibly operates in more standard proto–neutron star neutrino-driven winds, as well as during neutron star mergers, similar to the limited r-process. But overall, the initial conditions are fundamentally different for the νp -process, as it requires a proton- and $\overline{\nu}_e$ -rich environment with $Y_e > 0.5$.

Having the limited r-process operate in core-collapse supernovae has a number of advantages. If the main r-process makes second- and third-peak elements, then the first-peak element variations found in r-process-enhanced stars could be understood in terms of supernovae providing variable amounts of light neutron-capture elements to the gas from which these stars formed. Consequently, the observed patterns of r-process-enhanced stars must be a superposition of the yields of the limited and the main r-processes. In addition, the supernovae would also be responsible for the lighter fusion elements observed in r-process-enhanced metal-poor stars. Also, since all other ordinary metal-poor stars contain at least small amounts of neutron-capture elements (118), the associated huge variations at a given metallicity could be better understood if supernovae provide this material as part of an ongoing chemical evolution. An important question is whether an isolated, clean signature of the limited r-process might be observable, beyond the hints of its existence provided by r-process-enhanced stars and their first-peak deviations. The best candidate is the neutron-capture-element-poor star HD122563 (119), which exhibits a relative overabundance of light, first-peak neutron-capture elements compared with heavier ones (where the overall level of enrichment is rather low, commensurate with the low neutron-capture abundances found in metal-poor stars). However, while rapid neutron capture provides a plausible partial explanation, a significant contribution to elements with $Z \gtrsim 38$ at early times is also predicted to come from massive (>8 M_{\odot}) stars, by charged-particle reactions associated with QSE in core-collapse supernovae and/or by the s-process (47, 63).

Additional theoretical, experimental, and observational studies are needed to better understand the details of different r-process contributions, their sites, and their impact on chemical evolution, including understanding how r-process calculations are affected by uncertainties in the

nuclear properties (e.g., masses, neutron-capture cross sections, β decay rates) and the astrophysical conditions that enable nucleosynthesis (e.g., Y_e , temperature, density, and expansion timescales) (109). In particular, uncertainties in the masses of neutron-rich nuclei influence reaction rates, the r-process path, and the fission region (and thus second-peak properties and other freeze-out effects). Regardless, it is likely that multiple or even all of the r-process components listed in **Table 2** are ultimately required to fully explain the complete neutron-capture-element abundance patterns in r-process-enhanced stars, including the deviations of the light neutron-capture elements with respect to the scaled solar r-process pattern.

3.4.4. Yet another site? The actinide boost stars. Some 30% of r-II stars exhibit unusually high thorium (and uranium) abundances (120), compared with the other stable r-process elements such as europium, leading to increased abundance ratios that are three to four times higher than those of other r-process-enhanced stars. Interestingly, since the actinide elements appear to be equally affected (121) by this phenomenon, the ratio of uranium to thorium still provides a reasonable age of 14 billion years for CS 31082-001, even though its ratio of thorium to europium suggests a negative age (see Section 3.4.5). This behavior has been termed an actinide boost (122). Its origin remains unknown, but speculations include multiple r-process sites with different conditions (92, 114). Interestingly, the brightest star in Reticulum II shows actinide deficiency, which further adds to this discussion (see Section 4.1). Regardless of whichever conditions and/or astrophysical r-process site(s) are operating, the frequent occurrence of the actinide boost stars will somehow need to be explained.

3.4.5. Nucleochronometric age dating of the oldest stars. The heaviest long-lived elements made in the r-process are the radioactive isotopes 232 Th and 238 U. Thorium has a half-life of 14 billion years; uranium, 4.5 billion years. The abundance of thorium, as well as that of other stable r-process elements including europium, can be readily measured in the spectra of r-process-enhanced stars. Uranium, by contrast, is very challenging to detect, given the weakness of the one available optical line, which is also severely blended by other absorption features. In order to date the event that created these isotopes, the abundance ratio of a radioactive element (i.e., thorium, uranium) to a stable r-process element (e.g., europium, osmium, iridium) is compared with the respective initial r-process production ratio (115, 122), a process analogous to dating archaeological artifacts through radiocarbon analysis. Ages can be calculated with the following equations (95):

$$\Delta t = 46.78 \times [\log(\text{Th}/r)_{\text{initial}} - \log \epsilon(\text{Th}/r)_{\text{now}}],$$

$$\Delta t = 14.84 \times [\log(\text{U}/r)_{\text{initial}} - \log \epsilon(\text{Th}/r)_{\text{now}}],$$

$$\Delta t = 21.76 \times [\log(\text{U}/\text{Th})_{\text{initial}} - \log \epsilon(\text{Th}/r)_{\text{now}}].$$

In this manner, approximately 20 r-process-enhanced stars with thorium detections have been dated to $\Delta t = 10$ –14 billion years, depending on which abundance ratio was employed (89, 94, 123–125). Regarding uranium, only five stars have reliable abundance measurements (95, 96, 115, 126). **Figure 6** shows the spectral region around the weak uranium line in HE 1523–0901, which is currently the most reliable uranium measurement. Ideally, we want abundances of both radioactive elements to be available to produce a uranium-to-thorium ratio, as well as many ratios with the stable elements so that ages from all the different ratios can be calculated. As can be seen from the equations, the thorium-to-r ratio is the least accurate. The uranium-to-thorium ratio should be less susceptible to uncertainties in the nuclear physics inputs required to calculate the production ratio. Uncertainties are expected to largely cancel out because the two elements

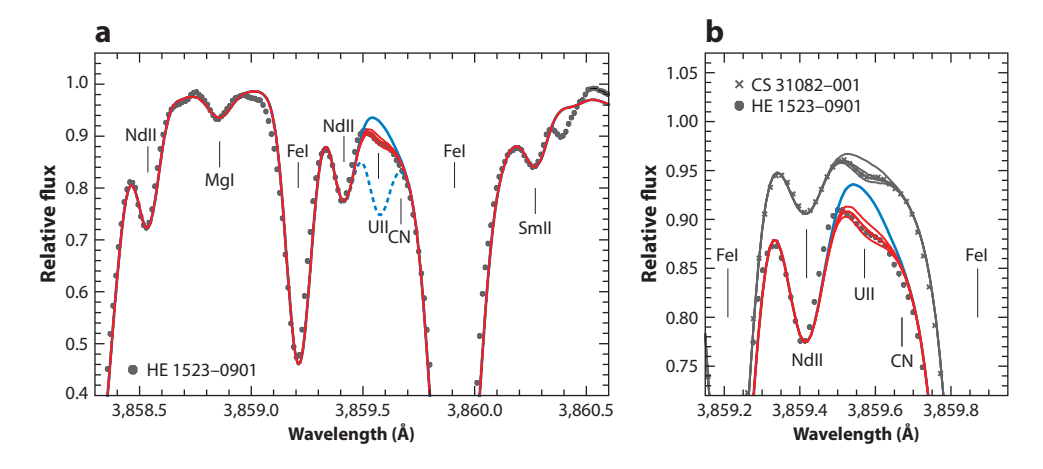


Figure 6

Spectral region around the U II line at 385.9 nm in (*a*,*b*) HE 1523-0901 (*black dots*) and (*b*) CS 31082-001 (*crosses*). Overplotted are synthetic spectra with different uranium abundances (*red*). The thin blue dotted line in panel *a* represents the line strength if uranium had not decayed, whereas the blue line indicates its absence. Adapted from Reference 129.

have nearly the same atomic mass (127, 128). For the same reason, the heaviest stable elements from the third r-process peak region (osmium, iridium) are more desirable to use for age dating than the lighter ones, such as europium. This is somewhat unfortunate, since europium is the most easily measured element of those typically used for age dating. Accordingly, stars with both thorium and uranium are the rarest but also the most desirable r-process-enhanced stars. Unfortunately, realistic age uncertainties range from approximately two to five billion years, depending on which ratio is used (see References 122 and 129 for more detailed discussions).

Another general issue with existing production ratios is that they are based on r-process calculations tailored to supernovae being the astrophysical site of the r-process, or are simply site-independent calculations. Neither may be a good match, not only because neutron star mergers are likely the primary production site (Section 4) but also because production ratios might be unique for each event. Multiple r-process-enhanced stars indicate that this is the case (93, 115); more theoretical research is clearly required to obtain accurate and precise stellar ages from this approach.

The good news is that the many different r-process models, all based on various assumptions out of necessity, can principally be self-consistently constrained by r-process-enhanced stars if abundances of all three of the elements thorium, uranium, and lead are available. These elements are intimately coupled not only to one another but also to the conditions under which they were formed. Lead is the β plus α decay end product of all decay chains in the mass region between lead and the onset of dominant spontaneous fission in the transuranian region. In addition, a portion of it is produced by the decay of uranium isotopes (and, less so, by thorium). The isotope 238 U decays into 206 Pb, 232 Th into 208 Pb, and 235 U into 207 Pb (where the last one is based on a theoretically derived ratio of 235 U/ 238 U). Thus, the known abundances of all three elements provide the only available observational constraint on the still poorly understood actinide production. Models of the r-process will need to be able to successfully reproduce these three abundances.

These same models might also be used to provide improved initial production ratios that could then increase the accuracy of stellar age dating. Currently, two r-II stars have lead measurements available, CS 31082-001 (130) and HE 1523-0901 (A. Frebel et al., manuscript in preparation);

only a few of the r-process-enhanced stars are suitable for abundance measurements of thorium, uranium, and lead. These elements have their strongest optical lines at 401.9 nm, 385.9 nm, and 405.7 nm, respectively. Overall, the cooler the star is, the stronger the absorption lines appear in the spectrum (at fixed abundance). Of course, increasing the elemental abundance also increases the line strengths, which is generally desirable when attempting to measure elements that have only weak atomic transitions. Many neutron-capture-element lines are in fact very weak and blended, and thus require exceptionally high-quality spectra (R > 60,000 with a signal-to-noise ratio S/N > 350 per pixel at 390 nm for uranium measurement, and $S/N \sim 500$ at 400 nm for lead). In addition, the carbon abundances should be low (ideally, subsolar) to minimize blending of all three lines with CH and CN features; otherwise, measurements are not possible. Finally, bright (preferably V < 13 magnitudes) metal-poor giants are most desirable in this regard, in order to collect the required spectra in reasonable observing time. As more bright r-process-enhanced stars are discovered (82, 83), at least a few more lead measurements can hopefully be attempted soon.

Regardless of all these challenges, the old ages derived for r-process-enhanced stars qualitatively confirm that low-metallicity stars are indeed ancient, and formed shortly after the Big Bang. In the absence of a reliable age-metallicity relation for halo stars, this finding implies that other metal-poor stars without any r-process enhancement are also old, as there is no discernible difference in the light-element abundances of r-process-enhanced stars and those of ordinary metal-poor stars. After all, r-process-element production is independent from that of the light fusion elements. The common assumption about low mass $(0.6-0.8\ M_{\odot})$ implying a star's current old age also appears justified, and the concept of stellar archaeology, namely that metal-poor stars are suitable for studying the conditions of the early Universe, is broadly validated. In addition, the 10-14-billion-year-old r-process-enhanced stars provide a lower limit on the age of the Milky Way and the Universe itself. An age of the Universe of 13.8 billion years has been derived from observations of the cosmic microwave background radiation, as interpreted with the latest cosmological models (131). Prior to the discovery of r-process-enhanced stars and precision cosmology, globular clusters were thought to be the oldest observable objects, with ages around 12-16 billion years. This was roughly in line with the age of the Universe known at the time.

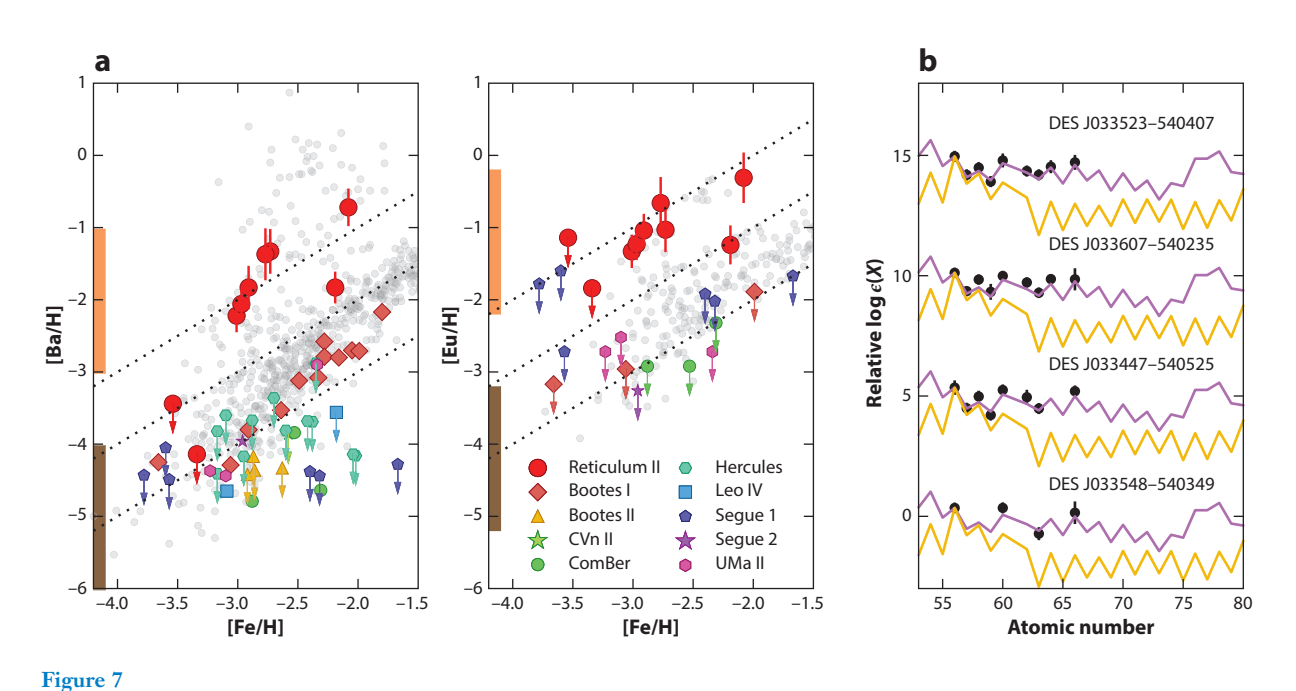
4. DWARF GALAXIES AS NUCLEAR PHYSICS LABORATORIES

A cornerstone of nuclear astrophysics is establishing the astrophysical sources and sites of heavyelement production. Research on r-process-enhanced metal-poor stars has long provided detailed insight into the fact that the r-process must have already occurred in the early Universe, but likely only sporadically, given the small fraction of r-process-enhanced stars. We also learned that it produces a universal pattern among the heavy neutron-capture elements and that challenges exist in the first-peak region and in relation to the actinides. The next step will be to employ astrophysical evidence to gain insight into where this process occurs, as the halo stars, with their (individually) unknown origins, cannot provide this information. Whereas the sites of all other major nucleosynthesis processes are relatively well understood, the astrophysical production site of the r-process has been debated for 60 years (85, 132). Candidate sites must produce a strong neutron flux, so naturally only the most violent events, such as supernova explosions or merging neutron stars, can be considered. Moreover, the low metallicity of r-process-enhanced stars requires relatively fast enrichment prior to their formation. This fact has been used (7, 8) to argue for supernovae, as they provide prompt enrichment. Moreover, supernovae are responsible for all of the lighter fusion elements observed in metal-poor stars, but tension with theoretical heavy-element production models could not be resolved (133, 134). The recent discovery of the first r-process galaxy, Reticulum II, initiated a drastic reinterpretation of the astrophysics data and

confirmed the importance of dwarf galaxy archaeology: The stars in this dwarf galaxy suggest that the r-process occurs predominantly in neutron star mergers.

4.1. The r-Process Galaxy Reticulum II

Reticulum II is a small, ultrafaint ($L \sim 3,000 L_{\odot}$) dwarf galaxy located in the Galactic halo at a distance of only 30 kpc from the Galactic center, discovered in data from the Dark Energy Survey (DES) (135, 136). Like all other ultrafaint dwarfs, it contains only a few thousand stars, but is highly dark matter dominated (137), remarkably metal poor ([Fe/H] = -2.65), extremely old [12 billion years, according to its color-magnitude diagram (138)], and devoid of gas. Chemical abundance studies based on high-resolution spectroscopy have confirmed that stars in Reticulum II are indeed chemically primitive (87, 139), lending support to the idea that ultrafaint dwarf galaxies have preserved the signatures of the earliest metal-production events in the Universe, and at least some of them may be first/early galaxies that somehow survived to the present day (48, 140, 141). Furthermore, these observations revealed that seven of the nine brightest stars under investigation exhibit an unusual, extreme enhancement in r-process elements (compared with most halo and all other dwarf galaxy stars) and that their abundances match the scaled solar r-process pattern above barium—they are all r-II stars (**Figure 7**). Previously, this signature had only been observed in the Milky Way r-process-enhanced halo stars, as described above. Reticulum II is therefore the first known r-process galaxy. It must have experienced a seemingly rare and prolific r-process event, given that this signature was found only in 1 of 10 ultrafaint dwarf galaxies that had at least one star studied with high-resolution spectroscopy at that time. Note that, since stars in the other



(a) Barium and europium abundances of stars in Reticulum II (red points), in the halo (gray), and in ultrafaint dwarf galaxies (colored points) as a function of iron abundance. Orange and brown vertical bars indicate yield ranges predicted by a neutron star merger and a core-collapse supernova, respectively. Arrows denote upper limits. (b) Observed abundances overlaid with the scaled solar r- and s-process patterns, shown in purple and gold, respectively. Adapted from Reference 87.

nine ultrafaint dwarfs show abundances of neutron-capture elements that are unusually low, this finding was doubly surprising.

The enhanced abundances of elements associated with the main r-process clearly point to a neutron star merger as responsible for the enrichment in Reticulum II (87, 93, 142). Interestingly, prior to the discovery of Reticulum II, neutron star mergers were not believed to be suitable as main r-process-element producers, at least not in the early Universe. At face value, the low metallicity of r-process-enhanced halo stars suggested a fast enrichment channel, more easily provided by supernovae. But this approach could not factor in any information about the halo stars' birth environment, as their origins are unknown. All of the stars in Reticulum II, however, come from the same dwarf galaxy. Consideration of environmental information, such as what might have occurred in a young Reticulum II, showed that approximately 100 million years are needed for the gas in such a small system to cool down sufficiently to form the next generation of stars (143), following a major energy injection by the explosion of the very first stars. Luckily, this time span appears long enough for a neutron star binary to in-spiral and merge (144). Adding up the yields of hundreds to thousands of supernovae to reach the same enrichment level as that of a neutron star merger, as an alternative, would instead cause disruption of the system. In addition, one can estimate the gas mass of Reticulum II, into which the yield of the r-process event was diluted. A minimum gas mass of $10^5 \, \mathrm{M}_{\odot}$ is given by the amount of swept-up gas in a supernova explosion (87), as well as by the mass of typical star-forming clouds (145). The total luminous (baryonic) mass of Reticulum II, $10^7 M_{\odot}$, provides an upper bound. The expected abundance level for stars to form from the enriched gas was derived (assuming homogeneous and instantaneous metal mixing) from yield predictions of theoretical calculations of r-process nucleosynthesis occurring in neutron star mergers (103). The results agree well with the observed data for stars in Reticulum II. Note that the observational results would also agree with the yields from magnetorotationally driven jet supernovae, but recent results suggest that these yields might be significantly lower than previously thought (113).

Regarding Reticulum II, of course some supernovae could have exploded, at least as part of the first generation of stars. A limited r-process likely took place in these explosions, providing small amounts of neutron-capture elements to the system (see Section 4.4 for more details). In Reticulum II, such marginal enrichment could explain the nature of the two stars found that do not display r-process enhancement but, rather, extremely low neutron-capture-element abundances. Sequential bursts of star formation might have produced the neutron-capture-poor stars first (they have slightly lower [Fe/H]) before the neutron star merger took place, after which the r-process-enhanced stars formed. Alternatively, inhomogeneous mixing might explain the abundance variations, or Reticulum II could have absorbed another small dwarf galaxy, which would imply that the neutron-capture-poor stars actually formed outside of Reticulum II. The latter scenario is appealing because the stars found in all other ultrafaint dwarf galaxies have equally low heavy-element abundances as these two stars.

Another aspect to consider is the light neutron-capture elements in Reticulum II stars. As shown in **Figure** 5b, these stars have some of the lowest and most discrepant first-peak abundances (strontium-yttrium-zirconium) compared with the solar r-process pattern, when scaled to elements barium and higher. These deviations are further discussed for halo stars in Section 3.4.3, but it is interesting to specifically consider them in the context of Reticulum II. Recall that the main r-process leads to the production of second- and third-peak elements, but likely no first-peak elements. Since Reticulum II is the chemically cleanest environment yet found in which a neutron star merger occurred, the stable r-process pattern for elements barium and above can easily be explained in this way (see also the discussion above). What is observed in the first peak, however, must result from the supernovae that exploded in the system, with a limited r-process operating.

The r-process-enhanced stars that exhibit large first-peak deviations, such as CS 22892-052 (94), might have originated from clean systems such as Reticulum II. Other r-process-enhanced stars with less-deviant abundances might correspondingly have formed from larger, more massive galaxies that underwent some level of chemical evolution (i.e., experienced a greater number of supernovae). Overall, the above scenario might explain the full range of variations among r-process-enhanced halo stars, including the solar pattern, given the variable number of supernovae that a host system experienced. While more theoretical studies are needed, these observations should principally be able to constrain the supernova population and the limited r-process. Interestingly, new observations (93) have shown the brightest star in Reticulum II to be an actinide-deficient star (see Section 3.4) because it has a lower-than-expected thorium abundance. High-quality data could be obtained for this star, but the others are too faint. Thus, it will remain a question for some time whether the other r-process-enhanced stars in this galaxy also exhibit actinide deficiency. The answer to this question could provide an important constraint on r-process nucleosynthesis, including whether different components of a neutron star merger could explain this phenomenon.

Dwarf galaxy archaeology (i.e., observing stars in dwarf galaxies) has one clear advantage. Given the known origin of these stars, the entire system can be theoretically modeled and thus better interpreted in terms of its chemical evolution and star formation history. The clear downside is the huge amount of large-aperture telescope time required (typically one night per star) to observe these distant, and thus relatively faint, stars. Multifiber echelle spectrographs alleviate this issue somewhat by enabling observations of multiple (approximately 10) stars at once, but even then, only the very brightest stars can be studied with current telescope and detector technology. Among r-process-enhanced halo stars, by contrast, very bright metal-poor objects can be selected (itself a long-term effort), for which it is comparatively easier to obtain exquisite data quality, so that many elements, including uranium and lead, can be measured. But the disadvantage of these stars remains their unknown individual origins.

An overall comparison of r-process-enhanced halo stars with those found in Reticulum II shows that their absolute (i.e., relative to hydrogen) enhancement levels match, suggesting a common origin in dwarf galaxies. Variations in the enhancement could simply be due to the amount of gas present in the various dwarf galaxies into which r-process elements are diluted. Observational constraints from additional r-process dwarf galaxies, as well as simulations of galaxy assembly, should soon provide more information about how these two populations are linked. The discovery of Reticulum II underpins the importance of the astrophysics component, which is complementary to experimental nuclear physics efforts that obtain measurements, or very good predictions, of the fundamental properties (e.g., masses, nuclear interaction cross sections, and decay rates) of heavy neutron-rich nuclei. These efforts are a prime motivation for several international accelerator facilities, such as FRIB, now under construction at Michigan State University (expected completion in 2022), and others proposing similar research, such as FAIR (Germany), RIKEN (Japan), and RAON (South Korea). Until many of the current nuclear physics uncertainties in r-process nucleosynthesis networks are resolved, interpretation of the abundance patterns of r-processenhanced stars needs to be carried out mindfully, so as not to ascribe any apparent discrepancies with models to properties of the astrophysical site.

4.2. Other Dwarf Galaxies with r-Process-Element Signatures

Soon after the discovery of Reticulum II, a second r-process galaxy was identified. The brightest star in the somewhat more massive ultrafaint dwarf galaxy Tucana III was observed with high-resolution spectroscopy. It exhibits a moderate r-process enhancement; in other words, it is an r-I star (146). For elements above barium, the element pattern matches that of the scaled solar

r-process, whereas first-peak elements deviate, as in the Reticulum II stars. Additional Tucana III stars show similar enhancements (J. Marshall, personal communication). Tucana III is believed to have been even more massive in the past, which might explain why its r-process level is lower than that found in Reticulum II, as any yield would likely have been more diluted.

A handful of r-II stars (classified on the basis of their [Ba/Eu] ratio) were previously found in the more massive classical dwarf galaxies Ursa Minor, Draco, and Fornax (see Reference 146 for more details). Approximately 20 r-I stars had also been identified in Draco, Ursa Minor, Sculptor, Fornax, and Carina (147–149). While not all of these perfectly match the scaled solar r-process pattern (or simply do not have enough abundance measurements available to test for a match), observation of signs of r-process nucleosynthesis implies that enrichments from neutron star mergers may be rare but not unique, and are not restricted to ultrafaint dwarf galaxies. The observed variations in absolute r-process enhancements in all of these systems might be due to different dilution masses, the timing of the neutron star merger, subsequent chemical evolution and star formation history, and/or unique accretion histories. In this context, Draco is of particular interest. Its stars cluster around certain metallicities such that each cluster shows distinctly different [Ba/Fe] ratios, possibly due to multiple events or processes that enriched Draco with time (149).

4.3. The Gravitational-Wave Connection

The LIGO and Virgo observatories recently detected, for the first time, the gravitational-wave signal of a neutron star merger, GW170817 (150, 151). Its electromagnetic counterpart, SSS17a, was also observed (152, 153); this event is known as a kilonova, and is believed to be the radioactive decay afterglow following the production of unstable heavy neutron-rich isotopes during an r-process event. For stellar archaeology, the significance of this detection lies in the assumption that the r-process-enhanced stars in Reticulum II (as well as other r-process-enhanced halo stars) are probing the ejecta of events such as GW170817. The detailed abundances of r-process-enhanced stars provide important constraints on the nature of r-process event(s) that occurred in the early Universe. This is complementary to gravitational-wave science, which is now able to provide specific data on the astrophysical site of the r-process in the local Universe, and to deep-sea measurements of plutonium deposited there by local r-process event(s) (154).

In light of these two avenues, neutron star mergers appear to produce r-process elements throughout cosmic history. But several open questions remain to be addressed. The frequency of occurrence, both locally and in the early Universe, is needed to incorporate neutron star mergers into chemical evolution models in order to broadly probe them as being the dominant r-process-element producers. At present, the inferred neutron star merger rate is $R_{\rm NSM} = 1,540^{+3,200}_{-1,220}~{\rm Gpc}^{-3}$ year $^{-1}$ (150), for a core-collapse supernova rate of $R_{\rm CCSN} \approx (1.1 \pm 0.2) \times 10^5~{\rm Gpc}^{-3}~{\rm year}^{-1}$ (155). For Reticulum II, Ji et al. (87) estimated that one neutron star merger would have occurred for every \sim 2,000 core-collapse supernovae. Clearly, no exact agreement has yet been reached, as the GW170817-based estimates are a factor of \sim 10 higher than what the Reticulum II case suggests. As more neutron star mergers and r-process dwarf galaxies are detected, these values are expected to rapidly improve.

The r-process yield of each event is also crucial to quantify. The total mass ejected by GW170817 is $\sim 0.05~{\rm M}_{\odot}$, which may correspond to $\sim 10^{-5}~{\rm M}_{\odot}$ of europium per event (156). This value is not unlike what was found to match observations of the stars in Reticulum II: $M_{\rm Eu} \sim 10^{-4.5\pm1}~{\rm M}_{\odot}$ (87). Nevertheless, yields need to be obtained for many neutron star mergers to determine whether there is a universal yield, or whether individual properties of neutron star mergers and/or their binary and merger dynamics lead to yield variations. Modeling the

r-process in neutron star mergers will then become much more detailed. However, theoretical yield calculations remain difficult, but could be dramatically aided by improved nuclear properties of the isotopes involved in *r*-process nucleosynthesis. New facilities such as FRIB will address these important shortcomings, as the results and implications are of interest to many subfields within astronomy and astrophysics. Along the way, model results will continue to be constrained with observations of *r*-process-enhanced halo stars and *r*-process galaxies to reach a more complete understanding of the origin of the heaviest elements.

4.4. Chemical Evolution of Neutron-Capture Elements and the Galaxy Formation Connection

The r-process-enhanced stars constitute only a small fraction of metal-poor stars (89). All other halo stars exhibit (118) at least a low abundance of neutron-capture elements (typically measured for strontium and barium), although they do not show any characteristic abundance patterns that would point to a specific origin of these elements (see References 7 and 8 for more details) (**Figure 8**). Generally, at the lowest metallicities, neutron-capture-element abundances are highly depleted, indicating early production of small amounts of these elements that were then contributed to the natal gas clouds of these stars. In particular, stars in ultrafaint dwarf galaxies show extremely low abundances (except those in r-process galaxies) (48). These observations point to the limited r-process as a likely source, since it could operate in any supernova or supernovae whose progenitors' mass falls in a specific range (157), at least at the earliest times. Rapidly rotating massive stars, however, might also produce these elements (47). The steep increase of, for instance, [Sr/Fe] at [Fe/H] \sim -3 points to an increase in neutron-capture elements independent of iron and other light elements. Then, from [Fe/H] \sim -2.6, the s-process contributes these elements as

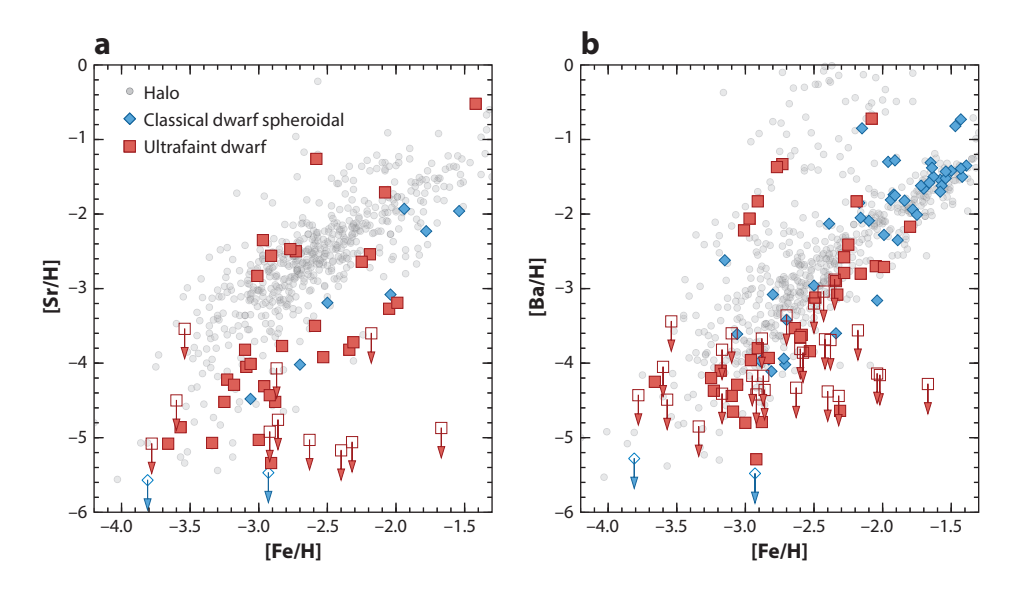


Figure 8

Evolution of the abundances ([X/H]) of neutron-capture elements (a) strontium and (b) barium as a function of the iron abundance. Halo stars and stars from classical dwarf spheroidal and ultrafaint dwarf galaxies are shown. Upper limits are indicated with arrows. Figure adapted from image by A. Ji.

well, and the evolution of strontium and barium proceeds in lockstep with that of lighter elements. Theoretical modeling of the observed abundance trends of various neutron-capture elements has been challenging (158), but the addition of yields from neutron star mergers to Galactic chemical evolution models and hydrodynamical simulations of galaxy formation has proven very promising (159–162).

From a broader perspective, our Galaxy formed from the accretion of smaller galaxies and building blocks, especially at the earliest times. The oldest stars found today in the Milky Way must date back to the earliest star-forming events, and thus likely originated in some of these small, early galaxies. These were later absorbed into the Milky Way, spilling all their stars into the outer region—the stellar halo—of our Galaxy. As a consequence, any information on the original host galaxy, in which the stars formed, is lost. Applying this scenario to r-process-enhanced stars suggests that they may well have formed in now-accreted systems that were very similar to Reticulum II. After all, these halo stars are very ([Fe/H] < -2) and extremely ([Fe/H] < -3) metal poor, and their r-process patterns and levels of enrichment strongly resemble those of the r-process-enhanced stars in Reticulum II. Thus, a common birth environment is likely, implying that characteristic abundance patterns, such as that of the r-process, could be used to trace the hierarchical buildup of the Milky Way. More specifically, it might become possible to use the population of r-process-enhanced halo stars as tracers of the fraction of early accreted dwarf galaxies that built the halo of the Milky Way. This broadly follows the idea of chemical tagging, initially envisioned by Freeman & Bland-Hawthorn (11), who suggested that the Galaxy's formation history is encoded in the chemical abundances of its stars.

To make this approach a reality, a census of all r-process-enhanced stars in both the Galaxy and dwarf galaxies needs to be undertaken. New observational efforts to identify additional r-process-enhanced halo stars are already under way (19, 82, 83, 126). Through the use of a variety of telescopes in both hemispheres, more than a dozen new r-II stars have been identified in the last 1–2 years alone; this effort aims to build up a sample of a total of \sim 100 known r-II stars. Only in this way can we obtain statistically significant results that will provide a legacy data set for constraining theoretical and experimental r-process studies well into the era of experimental facilities such as FRIB. This research follows initial efforts (163) to increase the then-small number of known r-II stars to the current number of ~ 30 (89, 125), as well as to deliver several dozen r-I stars. Other previous efforts have found only a few r-II stars (e.g., 129, 164, 165); they also discovered stars with s- and i-process enhancement, or with a combined r+s signature, although in less systematic ways. In addition, as new dwarf galaxies are discovered, their brightest stars will be observed to check for r-process enrichment. New r-process galaxies are much needed to continue to establish the fraction of small systems that hosted a neutron star merger. This promising new avenue to study galaxy assembly with stellar chemical signatures is grounded in our current understanding of the nuclear physics of element production; only with concerted efforts on both the nuclear physics and astrophysics fronts can it reach its full potential.

The r-process-enhanced stars have previously been called the cosmic Rosetta Stone for deciphering the origin of the r-process. This concept should now be extended to the truly remarkable r-process galaxies, as they bring together seemingly different research areas ranging from nuclear physics to gravitational physics and astrophysics in a unique and fascinating way. This convergence, and the progress made through the gravitational-wave detections, new nuclear accelerator facilities (under construction), and many theoretical and observational efforts, promises to finally resolve the remaining, extremely challenging questions about the r-process. Increasingly strong constraints on the nature of the r-process and the identification of the astrophysical site of the r-process are thus imminent, and will usher in a full understanding of the origin of the heaviest elements in the cosmos.

FUTURE ISSUES

- 1. Observational astrophysics must continue to deliver suitable metal-poor stars in order to study the various nucleosynthesis processes. In particular, r-process-enhanced stars with detectable thorium and uranium will provide the most stringent constraints on the r-process. Research on metal-poor stars in additional dwarf galaxies (e.g., those yet to be discovered with DES and the Large Synoptic Survey Telescope) will provide complementary information to help identify the site(s) of the r-process. Once the elemental yields are known, the gas dilution masses could be derived from stellar abundances. Such results would provide crucial constraints for cosmological simulations of early galaxy formation. Additional s-, i-, and r + s-process-enhanced stars will provide the means to study the low to intermediate neutron-density regime, especially at low metallicity. This research needs to be combined with binary star mass-transfer modeling to correctly interpret the observed stellar abundances.
- 2. To ensure long-term success, better optical and near-UV spectra of already-known metal-poor stars are needed, along with improved atomic data, NLTE, and 3D stellar atmosphere modeling in addition to larger telescopes. Close collaboration between nuclear physics and stellar astronomy will be required to leverage next-generation telescopes, such as the 25-m Giant Magellan Telescope. When equipped with high-resolution spectrographs, these instruments have the potential to provide currently missing data to move observational nuclear astrophysics into a new era of discovery.
- 3. Only nuclear physics theory can provide detailed yield predictions of the various nucleosynthesis processes. Much needed are low-metallicity s- and i-process yields, as well as r-process yields taking potential sites with different components into account (e.g., neutron star mergers). It also remains to be determined how many and which neutron-capture elements can be produced by ordinary core-collapse supernovae. These yields are crucial for interpreting the observational data. In parallel, if enough r-process-enhanced stars are found that can be assumed to be of old age, initial production ratios could be determined empirically and compared with the theoretical predictions.
- 4. Nuclear physics experiments, such as the forthcoming FRIB, need to continue exploring the properties of nuclei far from stability in order to provide the fundamental physics inputs required for nucleosynthesis modeling. The success of nuclear astrophysics rests on our understanding of the basic properties of these nuclei.
- 5. Once all these achievements can be combined, it will be possible to finally understand where the r-process occurs in the Universe, why all r-II stars seemingly have the same [Fe/H] metallicity range, and why no r-process-enhanced star has yet been found with [Fe/H] < -3.5. A comprehensive understanding of the chemical evolution of r-process elements, along with the availability of low-metallicity s-process yields, will allow us to better understand the existence of CEMP-r + s stars. Together with supernova yields for the limited r-process, this will provide constraints on the overall chemical evolution of neutron-capture elements.

DISCLOSURE STATEMENT

The author is not aware of any affiliations, memberships, funding, or financial holdings that might be perceived as affecting the objectivity of this review.

ACKNOWLEDGMENTS

A.F. warmly thanks the JINA community for 15 years of fruitful discussions and enjoyable collaborations. She is indebted to Abdu Abohalima, Timothy Beers, Anirudh Chiti, Norbert Christlieb, Rana Ezzeddine, Alexander Ji, Amanda Karakas, Gail McLaughlin, John Norris, Vinicius Placco, Yong Qian, Ian Roederer, Hendrik Schatz, Joshua Simon, Rebecca Surman, and many others for sharing their passion about the origins of the elements in cosmos. Kaley Brauer, Melanie Hampel, Alexander Ji, and Amanda Karakas kindly provided figures. A.F. thanks the US Department of Energy's Institute for Nuclear Theory at the University of Washington for its hospitality during Program INT-17-2b and the Department of Energy for partial support during preparatory research for this review. A.F. thanks the participants of Program INT-17-2b for discussions that led to Table 2, especially Yong Qian. A.F. thanks the International Centre for Radio Astronomy Research (ICRAR) for its hospitality during the final stages of preparation of the review. She acknowledges support from the ICRAR Visiting Fellowship for Senior Women in Astronomy at the University of Western Australia and Curtin University, Perth, Australia. A.F. is supported by National Science Foundation CAREER grant AST-1255160 and acknowledges grant PHY-14-130152 (Physics Frontier Center/JINA Center for the Evolution of the Elements), awarded by the National Science Foundation. The writing of this review made use of NASA's Astrophysics Data System Bibliographic Services.

LITERATURE CITED

- 1. Payne CH. Stellar atmospheres; a contribution to the observational study of high temperature in the reversing layers of stars. PhD thesis, Radcliffe Coll., Cambridge, MA (1925)
- 2. Burbidge EM, Burbidge GR, Fowler WA, Hoyle F. Rev. Mod. Phys. 29:547 (1957)
- 3. Bland-Hawthorn J, Gerhard O. Annu. Rev. Astron. Astrophys. 54:529 (2016)
- 4. Frebel A, Norris JE. Annu. Rev. Astron. Astrophys. 53:631 (2015)
- Frebel A, Norris JE. In *Planets, Stars and Stellar Systems*, vol. 5, ed. TD Oswalt, G Gilmore, p. 55. Dordrecht, Neth.: Springer Sci. Bus. (2013)
- 6. Beers TC, Christlieb N. Annu. Rev. Astron. Astrophys. 43:531 (2005)
- 7. Sneden C, Cowan JJ, Gallino R. Annu. Rev. Astron. Astrophys. 46:241 (2008)
- 8. Jacobson HR, Frebel A. J. Phys. G 41:44001 (2014)
- 9. Fernández R, Metzger BD. Annu. Rev. Nucl. Part. Sci. 66:23 (2016)
- 10. Thielemann FK, Eichler M, Panov IV, Wehmeyer B. Annu. Rev. Nucl. Part. Sci. 67:253 (2017)
- 11. Freeman K, Bland-Hawthorn J. Annu. Rev. Astron. Astrophys. 40:487 (2002)
- 12. Bromm V, Coppi PS, Larson RB. Astrophys. 7. 564:23 (2002)
- 13. Feltzing S, Gonzalez G. Astron. Astrophys. 367:253 (2001)
- 14. Keller SC, et al. Nature 506:463 (2014)
- 15. Frebel A. Astron. Nachr. 331:474 (2010)
- 16. Starkenburg E, et al. Mon. Not. R. Astron. Soc. 465:2212 (2017)
- 17. Ness M, Freeman K. Publ. Astron. Soc. Aust. 33:e022 (2016)
- 18. Travaglio C, et al. Astrophys. 7. 601:864 (2004)
- 19. Gull M, et al. arXiv:1806.00645 [astro-ph] (2018)
- 20. Aoki W, et al. Astrophys. J. 655:492 (2007)
- 21. Placco VM, Frebel A, Beers TC, Stancliffe RJ. Astrophys. 7. 797:21 (2014)
- 22. Beers TC, Christlieb N. Annu. Rev. Astron. Astrophys. 43:531 (2005)
- 23. Aoki W, et al. Astrophys. 7. 655:492 (2007)
- 24. Yoon J, et al. Astrophys. 7. 833:20 (2016)
- 25. García Pérez AE, et al. Astron. 7. 151:144 (2016)
- 26. Tremblay PE, et al. Astron. Astrophys. 557:A7 (2013)
- 27. Sitnova TM, Mashonkina LI, Ryabchikova TA. Mon. Not. R. Astron. Soc. 461:1000 (2016)

- 28. Amarsi AM, et al. Mon. Not. R. Astron. Soc. 463:1518 (2016)
- 29. Ezzeddine R, et al. arXiv:1612.09302 [astro-ph] (2016)
- 30. Asplund M. Annu. Rev. Astron. Astrophys. 43:481 (2005)
- 31. Mashonkina L, et al. Astron. Astrophys. 528:A87 (2011)
- 32. Lind K, Bergemann M, Asplund M. Mon. Not. R. Astron. Soc. 427:50 (2012)
- 33. Bergemann M, et al. Mon. Not. R. Astron. Soc. 427:27 (2012)
- 34. Nordlander T, et al. Astron. Astrophys. 597:A6 (2017)
- 35. Gallagher AJ, et al. Astron. Astrophys. 593:A48 (2016)
- 36. Abohalima A, Frebel A. arXiv:1711.04410 [astro-ph] (2017)
- 37. Frebel A, et al. Nature 434:871 (2005)
- 38. Caffau E, et al. Nature 477:67 (2011)
- 39. Aguado DS, González Hernández JI, Allende Prieto C, Rebolo R. Astrophys. 7. Lett. 852:L20 (2018)
- 40. Arlandini C, et al. Astrophys. 7. 525:886 (1999)
- 41. Herwig F. Annu. Rev. Astron. Astrophys. 43:435 (2005)
- 42. Abia C, et al. Astrophys. 7. 579:817 (2002)
- 43. Gallino R, et al. Astrophys. J. 497:388 (1998)
- 44. Goriely S, Mowlavi N. Astron. Astrophys. 362:599 (2000)
- 45. Lugaro M, Karakas AI, Stancliffe RJ, Rijs C. Astrophys. J. 747:2 (2012)
- 46. Bisterzo S, et al. Astrophys. 7. 835:97 (2017)
- 47. Chiappini C, et al. Nature 472:454 (2011)
- 48. Frebel A, Simon JD, Kirby EN. Astrophys. 7. 786:74 (2014)
- 49. Hansen TT, et al. Astron. Astrophys. 588:A3 (2016)
- 50. Norris JE, Ryan SG, Beers TC. Astrophys. 7. 488:350 (1997)
- 51. Bisterzo S, et al. Mon. Not. R. Astron. Soc. 404:1529 (2010)
- 52. Busso M, Gallino R, Wasserburg GJ. Annu. Rev. Astron. Astrophys. 37:239 (1999)
- 53. Abate C, Pols OR, Izzard RG, Karakas AI. Astron. Astrophys. 581:A22 (2015)
- 54. Bisterzo S, et al. Mon. Not. R. Astron. Soc. 422:849 (2012)
- 55. Hampel M, Stancliffe RJ, Lugaro M, Meyer BS. Astrophys. 7. 831:171 (2016)
- 56. Aoki W, et al. Astrophys. 7. 561:346 (2001)
- 57. Ivans II, et al. Astrophys. 7. Lett. 627:L145 (2005)
- 58. Placco VM, et al. Astrophys. J. 770:104 (2013)
- 59. Karakas AI, Lattanzio JC. Publ. Astron. Soc. Aust. 31:e030 (2014)
- 60. Karakas AI. VizieR Online Data Cat. 740:31413 (2010)
- 61. Burris DL, et al. Astrophys. 7. 544:302 (2000)
- 62. Karakas AI, García-Hernández DA, Lugaro M. Astrophys. 7. 751:8 (2012)
- 63. Pignatari M, et al. Astrophys. 7. 710:1557 (2010)
- 64. Pignatari M, et al. Astrophys. 7. Lett. 687:L95 (2008)
- 65. Frischknecht U, Hirschi R, Thielemann FK. Astron. Astrophys. 538:L2 (2012)
- 66. Cohen JG, Christlieb N, Qian YZ, Wasserburg GJ. Astrophys. 7. 588:1082 (2003)
- 67. Barbuy B, et al. Astron. Astrophys. 429:1031 (2005)
- 68. Jonsell K, et al. Astron. Astrophys. 451:651 (2006)
- 69. Roederer IU, et al. Astrophys. 7. 679:1549 (2008)
- 70. Dardelet L, et al. arXiv:1505.05500 [astro-ph] (2015)
- 71. Cowan JJ, Rose WK. Astrophys. J. 212:149 (1977)
- 72. Herwig F, et al. Astrophys. 7. 727:89 (2011)
- 73. Roederer IU, Karakas AI, Pignatari M, Herwig F. Astrophys. J. 821:37 (2016)
- 74. Campbell SW, Lattanzio JC. Astron. Astrophys. 490:769 (2008)
- 75. Doherty CL, et al. Mon. Not. R. Astron. Soc. 446:2599 (2015)
- 76. Lugaro M, Campbell SW, de Mink SE. Publ. Astron. Soc. Aust. 26:322 (2009)
- 77. Jones S, et al. Mon. Not. R. Astron. Soc. 455:3848 (2016)
- 78. Denissenkov PA, et al. Astrophys. 7. Lett. 834:L10 (2017)
- 79. Cristallo S, Straniero O, Piersanti L, Gobrecht D. Astrophys. 7. Suppl. 219:40 (2015)
- 80. Campbell SW, Lugaro M, Karakas AI. Astron. Astrophys. 522:L6 (2010)

- 81. Fujiya W, et al. Astrophys. J. Lett. 776:L29 (2013)
- 82. Hansen TT, et al. Astrophys. 7. 858:92 (2018)
- 83. Sakari C, et al. Astrophys. 7. 854:L20 (2018)
- 84. Carney BW, et al. Astrophys. J. 125:293 (2003)
- 85. Burbidge EM, Burbidge GR, Fowler WA, Hoyle F. Rev. Mod. Phys. 29:547 (1957)
- 86. Cameron AGW. Annu. Rev. Nucl. Part. Sci. 8:299 (1958)
- 87. Ji AP, Frebel A, Chiti A, Simon JD. Nature 531:610 (2016)
- 88. Christlieb N, et al. Astrophys. J. 603:708 (2004)
- 89. Barklem PS, et al. Astron. Astrophys. 439:129 (2005)
- 90. Roederer IU, et al. Mon. Not. R. Astron. Soc. 445:2970 (2014)
- 91. Hansen TT, et al. Astron. Astrophys. 583:A49 (2015)
- 92. Hill V, et al. Astron. Astrophys. 387:560 (2002)
- 93. Ji AP, Frebel A. Astrophys. 7. 856:138 (2018)
- 94. Sneden C, et al. Astrophys. 7. 533:L139 (2000)
- 95. Cayrel R, et al. Nature 409:691 (2001)
- 96. Frebel A, Johnson JL, Bromm V. Mon. Not. R. Astron. Soc. 380:L40 (2007)
- 97. Simmerer J, et al. Astrophys. 7. 617:1091 (2004)
- 98. Roederer IU, et al. Astrophys. J. 724:975 (2010)
- 99. Roederer IU, et al. Astrophys. J. Lett. 747:L8 (2012)
- 100. Roederer IU, et al. Astrophys. 7. 675:723 (2008)
- 101. Gallagher AJ, et al. Astron. Astrophys. 538:A118 (2012)
- 102. Metzger BD, et al. Mon. Not. R. Astron. Soc. 406:2650 (2010)
- 103. Goriely S, Bauswein A, Janka HT. Astrophys. J. Lett. 738:L32 (2011)
- 104. Meyer BS, Krishnan TD, Clayton DD. Astrophys. J. 498:808 (1998)
- 105. de Mink SE, Belczynski K. Astrophys. J. 814:58 (2015)
- 106. Rosswog S, et al. Astron. Astrophys. 341:499 (1999)
- 107. Wanajo S, et al. Astrophys. J. Lett. 789:L39 (2014)
- 108. Lippuner J, Roberts LF. Astrophys. 7. 815:82 (2015)
- 109. Eichler M, et al. Astrophys. J. 808:30 (2015)
- 110. Korobkin O, Rosswog S, Arcones A, Winteler C. Mon. Not. R. Astron. Soc. 426:1940 (2012)
- 111. Wu MR, Fernández R, Martínez-Pinedo G, Metzger BD. Mon. Not. R. Astron. Soc. 463:2323 (2016)
- 112. Winteler C, et al. Astrophys. J. Lett. 750:L22 (2012)
- 113. Mösta P, et al. arXiv:1712.09370 [astro-ph] (2017)
- 114. Kratz KL, et al. Astrophys. J. 662:39 (2007)
- 115. Hill V, et al. Astron. Astrophys. 607:91 (2017)
- 116. Wanajo S, Kajino T, Mathews GJ, Otsuki K. Astrophys. 7. 554:578 (2001)
- 117. Qian YZ, Wasserburg GJ. Astrophys. 7. 588:1099 (2003)
- 118. Roederer IU. Astron. 7. 145:26 (2013)
- 119. Honda S, et al. Astrophys. 7. 643:1180 (2006)
- 120. Mashonkina L, et al. Astron. Astrophys. 516:46 (2010)
- 121. Roederer IU, et al. Astrophys. J. 698:1963 (2009)
- 122. Schatz H, et al. Astrophys. J. 579:626 (2002)
- 123. Johnson JA, Bolte M. Astrophys. 7. 554:888 (2001)
- 124. Cowan JJ, et al. Astrophys. J. 572:861 (2002)
- 125. Hayek W, et al. Astron. Astrophys. 504:511 (2009)
- 126. Placco VM, et al. Astrophys. J. 844:18 (2017)
- 127. Wanajo S, et al. Astrophys. 7. 577:853 (2002)
- 128. Kratz KL, Pfeiffer B, Cowan JJ, Sneden C. New Astron. Rev. 48:105 (2004)
- 129. Frebel A, et al. Astrophys. J. Lett. 660:L117 (2007)
- 130. Plez B, et al. Astron. Astrophys. 428:L9 (2004)
- 131. Planck Collab., et al. Astron. Astrophys. 594:A13 (2016)
- 132. Cameron AGW. Publ. Astron. Soc. Pac. 69:201 (1957)
- 133. Arcones A, Montes F. Astrophys. 7. 731:5 (2011)

- 134. Wanajo S. Astrophys. J. Lett. 770:L22 (2013)
- 135. Drlica-Wagner A, et al. Astrophys. J. 813:109 (2015)
- 136. Koposov SE, et al. Astrophys. J. 811:62 (2015)
- 137. Simon JD, et al. Astrophys. J. 808:95 (2015)
- 138. Bechtol K, et al. Astrophys. J. 807:50 (2015)
- 139. Roederer IU, et al. Astron. J. 151:82 (2016)
- 140. Frebel A, Bromm V. Astrophys. J. 759:115 (2012)
- 141. Chiti A, et al. Astrophys J. 857:74 (2018)
- 142. Ji AP, Frebel A, Simon JD, Chiti A. Astrophys. 7. 830:93 (2016)
- 143. Bland-Hawthorn J, Sutherland R, Webster D. Astrophys. J. 807:154 (2015)
- 144. Dominik M, et al. Astrophys. 7. 759:52 (2012)
- 145. Ji AP, Frebel A, Bromm V. Mon. Not. R. Astron. Soc. 454:659 (2015)
- 146. Hansen TT, et al. Astrophys. J. 838:44 (2017)
- 147. Shetrone M, et al. Astron. 7. 125:684 (2003)
- 148. Cohen JG, Huang W. Astrophys. J. 719:931 (2010)
- 149. Tsujimoto T, et al. Astrophys. 7. Lett. 850:L12 (2017)
- 150. Abbott BP, et al. Phys. Rev. Lett. 119:161101 (2017)
- 151. Abbott BP, et al. Astrophys. J. Lett. 848:L12 (2017)
- 152. Drout MR, et al. Science 358:1570 (2017)
- 153. Shappee BJ, et al. Science 358:1574 (2017)
- 154. Wallner A, et al. Nat. Commun. 6:5956 (2015)
- 155. Taylor M, et al. Astrophys. J. 792:135 (2014)
- 156. Côté B, et al. Astrophys. J. 836:230 (2017)
- 157. Lee DM, et al. Astrophys. J. 774:103 (2013)
- 158. Cescutti G, Chiappini C. Astron. Astrophys. 565:A51 (2014)
- 159. Tsujimoto T, Shigeyama T. Astrophys. J. Lett. 795:L18 (2014)
- 160. Cescutti G, et al. Astron. Astrophys. 577:A139 (2015)
- 161. Côté B, et al. Astrophys. J. 855:99 (2018)
- 162. Naiman JP, et al. Mon. Not. R. Astron. Soc. 477:1206 (2018)
- 163. Christlieb N, et al. Astron. Astrophys. 428:1027 (2004)
- 164. Lai DK, et al. Astrophys. J. 681:1524 (2008)
- 165. Aoki W, Beers TC, Honda S, Carollo D. Astrophys. J. Lett. 723:L201 (2010)



Annual Review of Nuclear and Particle Science

Volume 68, 2018

Contents

Guido Altarelli Luciano Maiani and Guido Martinelli	1
Multiquark States Marek Karliner, Jonathan L. Rosner, and Tomasz Skwarnicki	17
Penning-Trap Mass Measurements in Atomic and Nuclear Physics Jens Dilling, Klaus Blaum, Maxime Brodeur, and Sergey Eliseev	45
Dispersion Theory in Electromagnetic Interactions Barbara Pasquini and Marc Vanderhaeghen	75
Progress in Measurements of 0.1–10 GeV Neutrino–Nucleus Scattering and Anticipated Results from Future Experiments Kendall Mahn, Chris Marshall, and Callum Wilkinson	105
Structure of $S = -2$ Hypernuclei and Hyperon–Hyperon Interactions Emiko Hiyama and Kazuma Nakazawa	131
Deep Learning and Its Application to LHC Physics Dan Guest, Kyle Cranmer, and Daniel Whiteson	161
The Construction of ATLAS and CMS Michel Della Negra, Peter Jenni, and Tejinder S. Virdee	183
Small System Collectivity in Relativistic Hadronic and Nuclear Collisions <i>James L. Nagle and William A. Zajc</i>	211
From Nuclei to the Cosmos: Tracing Heavy-Element Production with the Oldest Stars Anna Frebel	237
Silicon Calorimeters JC. Brient, R. Rusack, and F. Sefkow	271
Automatic Computation of One-Loop Amplitudes Celine Degrande, Valentin Hirschi, and Oliver Mattelaer	291
On the Properties of Neutrinos A. Baha Balantekin and Boris Kayser	313

Heavy Ion Collisions: The Big Picture and the Big Questions Wit Busza, Krishna Rajagopal, and Wilke van der Schee	339
Particle Acceleration by Supernova Shocks and Spallogenic	
Nucleosynthesis of Light Elements	
Vincent Tatischeff and Stefano Gabici	377
Jefferson Lab at 12 GeV: The Science Program	
Volker D. Burkert	405
Dark Matter Searches at Colliders	
Antonio Boveia and Caterina Doglioni	429

Errata

An online log of corrections to *Annual Review of Nuclear and Particle Science* articles may be found at http://www.annualreviews.org/errata/nucl